On ultra-high energy cosmic ray acceleration at the termination shock of young pulsar winds

Martin Lemoine, Kumiko Kotera, Jérôme Pétri

Prepared for submission to JCAP

On ultra-high energy cosmic ray acceleration at the termination shock of young pulsar winds

Martin Lemoine[a] **Kumiko Kotera**[a] **Jérôme Pétri**[b]

[a]Institut d'Astrophysique de Paris,
CNRS, Université Pierre & Marie Curie,
98 bis boulevard Arago, F-75014 Paris, France
[b]Observatoire Astronomique de Strasbourg,
Université de Strasbourg, CNRS, UMR 7550,
11 rue de l'Université, F-67000 Strasbourg, France

E-mail: lemoine@iap.fr, kotera@iap.fr, jerome.petri@astro.unistra.fr

Abstract. Pulsar wind nebulae (PWNe) are outstanding accelerators in Nature, in the sense that they accelerate electrons up to the radiation reaction limit. Motivated by this observation, this paper examines the possibility that young pulsar wind nebulae can accelerate ions to ultra-high energies at the termination shock of the pulsar wind. We consider here powerful PWNe, fed by pulsars born with $\sim$ millisecond periods. Assuming that such pulsars exist, at least during a few years after the birth of the neutron star, and that they inject ions into the wind, we find that protons could be accelerated up to energies of the order of the Greisen-Zatsepin-Kuzmin cut-off, for a fiducial rotation period $P \sim 1\,\mathrm{msec}$ and a pulsar magnetic field $B_\star \sim 10^{13}\,\mathrm{G}$, implying a fiducial wind luminosity $L_\mathrm{p} \sim 10^{45}\,\mathrm{erg/s}$ and a spin-down time $t_\mathrm{sd} \sim 3\times 10^7\,\mathrm{s}$. The main limiting factor is set by synchrotron losses in the nebula and by the size of the termination shock; ions with $Z \geq 1$ may therefore be accelerated to even higher energies. We derive an associated neutrino flux produced by interactions in the source region. For a proton-dominated composition, our maximum flux lies slightly below the 5-year sensitivity of IceCube-86 and above the 3-year sensitivity of the projected Askaryan Radio Array. It might thus become detectable in the next decade, depending on the exact level of contribution of these millisecond pulsar wind nebulae to the ultra-high energy cosmic ray flux.

Keywords: Cosmic rays – Pulsar wind nebulae

Contents

1 Introduction

The origin of the highest energy cosmic rays is a long-standing enigma of astroparticle physics, which has withstood some fifty years of intense experimental activity (see reviews by, e.g., [1, 2]). The existing data have brought in very significant results, such as the detection of a cut-off at the expected location of the Greisen-Zatsepin-Kuzmin (GZK) suppression [3, 4]. Such a spectral feature, combined with the absence of striking anisotropy in the arrival direction of the highest energy particles, could indicate that they originate from extragalactic sources. So far, however, no conclusive experimental evidence points towards one or the other of the many possible scenarios of ultra-high energy cosmic ray (UHECR) origin.

The central question in this field of research is how to accelerate particles to these extreme energies $\sim 10^{20}\,$eV. Among the known particle acceleration scenarios, Fermi-type shock acceleration plays a special role. It is rather ubiquitous, since collisionless shock waves emerge as direct consequences of powerful outflows. Furthermore, shock acceleration, when operative, is known to dissipate into the supra-thermal particle population a substantial fraction of the kinetic energy that is inflowing into the shock, of the order of $\sim 10\%$, see e.g. [5]. Shock acceleration also produces rather generically a spectrum with nearly constant energy per decade, which allows to transfer a sizable fraction of the energy in the ultra-high energy domain. Those are noticeable features in the context of the origin of ultra-high energy cosmic rays, because one indeed needs to extract a large fraction of the source energy in order to match the cosmic ray flux above $10^{19}\,$eV, e.g. $E_{\rm UHECR} \sim 10^{53}\,\dot{n}_{-9}^{-1}\,$erg per transient source of ocurrence rate $\dot{n} = 10^{-9}\dot{n}_{-9}\,{\rm Mpc}^{-3}{\rm yr}^{-1}$ [6][1].

Particle acceleration to ultra-high energies in collisionless shock waves has been proposed in a number of scenarios [7], e.g. in gamma-ray bursts [8–12], in blazars [12, 13] or in radio-galaxy jets [13]. The possibility of accelerating ultra-high energy cosmic rays at the termination shock of pulsar winds has received so far little attention, except for Ref. [14], which

[1] Throughout the paper, quantities are noted $Q_x \equiv Q/10^x$ in cgs units, unless specified otherwise.

has stressed the large energy gain associated to the first shock crossings. The present paper thus proposes a critical discussion of this issue. Let us recall here that the ultra-relativistic collisionless shock front separates the (inner) cold fast magnetized pulsar wind from the pulsar wind nebula, which itself is bounded by a shock propagating into the supernova remnant; this nebula thus contains the hot shocked wind material and hot shocked supernova remnant material, e.g. [15–17].

The main motivation of the present study comes from the realization that the Crab nebula represents so far the most efficient particle accelerator known to us, since the observation of a synchrotron spectrum extending up to $\sim m_e c^2/\alpha_{\rm em}$ ($\alpha_{\rm em}$ the fine structure constant) attests of the capacity of the termination shock to accelerate electrons and positrons up to the radiation reaction limit at the Bohm rate, meaning an acceleration timescale $t_{\rm acc} \simeq \mathcal{A}\, t_{\rm g}$ in terms of the gyro-time $t_{\rm g}$, with $\mathcal{A} \sim 1$, expressed here in the comoving blast frame, e.g. [18]. Furthermore, it is generally admitted that the highest energy pairs have been shock accelerated through a Fermi process, because their spectral index $s \simeq 2.2$ is remarkably similar to the predictions of relativistic shock acceleration for isotropic scattering, see e.g. [19–23]. In this sense, it is natural to try to extend this result to the acceleration of ions. Of course, pulsar winds are usually modeled as pair winds, hence one central assumption of the present work is that such winds may also inject ions, see the discussion in Ref. [24], and see also [25–27] which propose to interpret the morphological features of the Crab Nebula through the coupling between ion and pair dynamics at the termination shock.

The confinement energy of cosmic rays in Crab-like nebulae is nevertheless quite low, being of the order of $E_{\rm conf} \simeq 3 \times 10^{17}\, B_{-3.5} R_{18.5}\, Z\, {\rm eV}$; here, B and R indicate respectively the magnetic field and the size of the blast. We will thus be interested in more powerful pulsar wind nebulae, able to confine particles up to higher energies. As we show in the following, young pulsars born with periods $P \sim 10^{-3}\,{\rm s}$ do fulfill this criterion; moreover, their huge rotational energy reservoir $E_{\rm rot} \simeq 10^{52}\, P_{-3}^2\, {\rm erg}$ is also highly beneficial for producing a substantial flux of UHECRs [28–31].

The release of this tremendous rotational energy into the surrounding supernova ejecta should modify its radiative properties. In particular, such objects could lead to ultra-luminous supernovae lasting for months to years, with distinctive bright gamma-ray and X-ray counterparts [32–36]. These scenarios could provide an explanation to some of the observed ultra-luminous supernovae [37], that would then constitute an indirect probe of the existence of pulsars born with millisecond periods. Interestingly, it has been suggested that the Crab pulsar itself was born with a 5 msec period on the basis of the observation of the large number of radio-emitting pairs in the nebula [38].

Engine-driven supernovae, or trans-relativistic supernovae, whose characteristic high speed ejecta is believed to be powered by some internal source such as a magnetized neutron star, have also been considered as potential sources of ultra-high energy cosmic rays [39–41]. However, in those scenarios, acceleration is argued to take place in the outer fastest parts of the mildly relativistic external shock which propagates in the wind of the progenitor star. Our present discussion proposes another view of these objects, in which particle acceleration to ultra-high energies takes place well inside the remnant, at the ultra-relativistic shock that is running up the pulsar wind.

Finally, young pulsar winds themselves have also been considered as potential sites of UHECR acceleration, mainly through the electric field associated to the rotating magnetic dipole, e.g. [24, 28–31, 42, 43]. We stress that the present scenario is wholly different in

terms of acceleration physics. In particular, pulsar magnetospheric and wind physics do not play any role in our scenario, beyond controlling the spin-down time of the engine, while it directly sets the maximum energy that might be reached in those wind acceleration models. In the present work, particle acceleration takes place in two steps: in a first step, the initial Poynting flux of the pulsar wind is assumed to be dissipated down to near equipartition with ions and electrons before or around the termination shock; this is a generic assumption, motivated by observational results on known pulsar wind nebula, e.g. [44, 45]; the injected high energy ions are then accelerated at the termination shock, up to a maximal energy determined by energy losses and escape considerations.

The lay-out of this paper is as follows. In Sec. 2, we discuss the dynamics and the radiative properties of the nebula, which limit the acceleration through radiative losses and escape, then we discuss the maximal energy as a function of the various parameters. In Sec. 3, we discuss the neutrino signal associated to the acceleration of ultra-high energy cosmic rays as well as the dependence of our results on the model assumptions and parameters. We provide a summary of our results and conclusions in Sec. 4.

2 Particle acceleration in young powerful PWNe

The physics of young PWNe is controlled by the amount of energy injected by the pulsar wind, of luminosity $L_{\rm w}(t)$, and the velocity-density profile of the supernova ejecta which confines the nebula. Detailed morphological studies of the Crab nebula, along with numerical MHD simulations [46, 47] indicate that the geometry is mostly axisymmetric. It is however possible to reproduce the main characteristics of a young pulsar wind nebula with a spherically symmetric picture, in particular the location of the termination shock radius and the size of the nebula, e.g., [42, 44]. Given the other astrophysical uncertainties described below, this suffices for our purposes and, in the following, we assume spherical symmetry.

Throughout this study, neutron stars have a moment of inertia $I_\star$ with fiducial value $10^{45}\,{\rm g\,cm^2}$, instantaneous and initial rotation velocities Ω and $\Omega_{\rm i}$ (corresponding initial period $P_{\rm i} = 2\pi/\Omega_{\rm i}$), radius $R_\star$ and dipole magnetic field $B_\star$; these should not be confused with magnetic field strengths and spatial scales of the nebula.

The pulsar rotational energy reservoir amounts to $E_{\rm rot} = I_\star \Omega_{\rm i}^2/2 \sim 2.0\times10^{52}\,{\rm erg}\, I_{\star,45} P_{\rm i,-3}^{-2}$. The wind luminosity decreases as

$$L_{\rm w}(t) = L_{\rm p}/(1+t/t_{\rm sd})^{(n+1)/(n-1)}\ , \tag{2.1}$$

in terms of the braking index n (defined by $\dot\Omega \propto \Omega^n$) and spin-down time $t_{\rm sd}$, with initial luminosity $L_{\rm p} \simeq E_{\rm rot}/t_{\rm sd} \simeq 0.64\times10^{45} P_{-3}^{-4} B_{\star,13}^2 R_{\star,6}^6\,{\rm erg/s}$. For magneto-dipole losses in the vacuum, $n=3$, while observations rather indicate $n\sim 2-2.5$. Nevertheless, we will be interested in the structure of the nebula at time $t_{\rm sd}$, at which a substantial fraction of the rotational energy has been output into the nebula; the braking index controls the later evolutionary stages, therefore it will not impact significantly our results. We thus adopt $n=3$ for simplicity in what follows.

The spin-down timescale is then given by

$$t_{\rm sd} \simeq \frac{9 I_\star c^3}{8 B_\star^2 R_\star^6 \Omega_{\rm i}^2} \sim 3.1\times10^7\,{\rm s}\, I_{\star,45} B_{\star,13}^{-2} R_{\star,6}^{-6} P_{\rm i,-3}^2\ . \tag{2.2}$$

For convenience, we indicate our results in terms of $B_\star$, $R_\star$ and P, as well as in terms of $L_{\rm p}$ and $t_{\rm sd}$.

We concentrate mainly on pulsars with magnetic fields $B \sim 10^{12} - 10^{13}\,\mathrm{G}$ and not on magnetars (with $B \gtrsim 10^{14}\,\mathrm{G}$). As Eq. (2.2) indicates, magnetars spin down on a timescale much shorter than a year, and at the early times when the highest energy particles are accelerated, the density of the surrounding supernova ejecta does not allow their escape [30]. A magnetar scenario thus require the disruption of the supernova envelope by the wind [24] or that particles escape through a region punctured by a jet, like in a strongly magnetized proto-magnetar scenario discussed by [48]. Gravitational wave losses are negligible for pulsars with $B \ll 10^{16}\,\mathrm{G}$, hence we neglect them, see e.g. [24].

2.1 General input from the Crab nebula

The extrapolation of the phenomenology of the Crab pulsar wind nebula to the young PWNe that we are interested in is by no means trivial, because it involves an increase by some six orders of magnitude in luminosity, and it is hampered by three unsolved issues: the so-called $\sigma-$problem, the physics of particle acceleration at the termination shock of pulsar winds and the origin of radio emitting electrons in PWNe. Let us recall briefly these issues in order to motivate our model of the nebula.

The magnetization parameter σ relates the Poynting flux to the matter energy flux; in the comoving wind frame, for a cold plasma of rest mass energy density nmc^2, it is defined by $\sigma \equiv B^2/\left(4\pi nmc^2\right)$. For a mixed pair-ion composition of respective densities κn_e and n_i, $nmc^2 \equiv n_\mathrm{i} m_\mathrm{i} c^2 + 2\kappa n_e m_e c^2$, κ defining the multiplicity factor for pairs achieved through pair cascade in the magnetosphere.

Observationally, the $\sigma-$problem results from the difficulty in reconciling the large value σ_0 of the magnetization parameter at the pulsar light cylinder with that inferred downstream of the termination shock (σ_PWN) through a leptonic model of the emission [18, 42, 44–46, 49]. A generic estimate for σ_0 in the Crab nebula is $\sigma_0 \sim \mathcal{O}(10^6)$, assuming that pairs are injected at the Goldreich-Julian rate (recalled further below), with a low energy, at the base of the wind, with multiplicity $\kappa \sim 10^4$. In contrast, models of pulsar wind nebulae and their comparison to observations rather suggest $\sigma_\mathrm{PWN} \sim 10^{-3} - 10^{-1}$ [44, 45, 50–53], although more recent three-dimensional MHD simulations suggest that values as large as $\sigma_\mathrm{PWN} \sim \mathcal{O}(1)$ could reproduce the morphological data for the Crab nebula [47, 54]. From a more theoretical perspective, this $\sigma-$problem characterizes the difficulty of pushing cold MHD winds to large Lorentz factors through the Poynting flux, e.g. [55–59]. Indeed, in a radially expanding MHD wind, σ should remain constant from close to the light-cylinder up to the termination shock.

How particle acceleration takes place in the Crab nebula is another puzzle. Although the termination shock offers an obvious site for particle acceleration, and the high energy spectral index $s \simeq 2.2$ of the reconstructed electron distribution $\mathrm{d}n/\mathrm{d}\gamma \propto \gamma^{-s}$ conforms well to the expectations of a relativistic Fermi process with isotropic scattering [19–23], so far our understanding of particle acceleration rather suggests that the Fermi process should be inefficient in mildly-magnetized – namely for a magnetization $\sigma \gtrsim 10^{-4}$ – ultra-relativistic shocks, see [60, 61] for an analytical discussion and [5] for simulations. To summarize such discussions briefly, Fermi acceleration can take place at ideal – meaning planar and steady – relativistic shock waves only if intense small-scale turbulence has been excited in the shock vicinity[2] [62]. Such small-scale turbulence may in principle be excited by streaming instabilities between the supra-thermal particles and the background unshocked plasma in

[2] small-scale means here $\lambda_{\delta B} < r_\mathrm{g}$, with r_g the gyroradius of accelerated particles

the shock precursor. At the termination shock of pulsar winds, this may come through a current-driven instability if $\sigma \lesssim 10^{-2}$ [63], or through the synchrotron maser instability, if $\sigma \gtrsim 0.1$ [25, 26]. Nevertheless, the finite magnetization, even if $\sigma_{\rm PWN}$ is as small as 10^{-3}, should prevent acceleration to very high energies, because the efficiency of scattering in small-scale turbulence relatively to the gyration in the background field decreases in inverse proportion to the particle energy [60, 64]. As discussed in these references, this implies a maximum energy beyond which scattering (hence acceleration) becomes ineffective. This maximum energy has been observed in recent PIC simulations [5]. Its exact value is not of importance for the present discussion; it suffices to say that it scales as $\sigma^{-1/2}$ so that, at mildly magnetized shock waves with $\sigma \gtrsim 10^{-4}$, Fermi acceleration should not be able to accelerate the particles to the energies observed, *in ideal conditions*.

Efficient dissipation of the magnetic field in the nebula, is probably the key to resolving both the $\sigma-$problem and the issue of particle acceleration. Regarding the former, recent 3D MHD simulations, which account for dissipative effects inside the nebula, alleviate somewhat the question of conversion of Poynting flux in the wind by allowing for values $\sigma_{\rm PWN} \sim \mathcal{O}(1)$ [47, 54]. Although the exact mechanism of dissipation remains open to debate, reconnection in the current sheet separating the "stripes" of opposite magnetic polarity (the "striped wind" [55, 65, 66]), upstream of the termination shock, has long been discussed as a possible way of converting part of the Poynting flux, e.g. [55, 67]. Dissipation around the termination shock may also support efficient particle acceleration in two ways: by seeding large scale turbulence, causally disconnected from the upstream magnetic topology, in which case particle acceleration could proceed unimpeded [62]; or, by providing an extra mechanism of particle acceleration, which would feed into the Fermi process at higher energies, e.g. through the dissipation of MHD waves [68], or reconnection [69–71]. Furthermore, the MHD simulations of Ref. [72] reveal that the termination shock is unsteady and corrugated, leading to the excitation of mildly relativistic turbulence immediately downstream. Finally, we also note that the high energy spectral index $s = 2.2$ is typical of a relativistic Fermi process in a mildly or weakly magnetized shock, whereas magnetized shock waves lead to a weaker compression ratio, hence a softer spectrum [20]. This, again, argues in the favor of substantial dissipation around the termination shock of the wind.

One can argue further in the favor of dissipation inside the pulsar wind nebula, as follows: ad absurdum, one could not construct a stationary model with a super-fast magnetosonic wind in the absence of dissipation [44], as the shock crossing conditions at the termination shock would then lead to a ultra-relativistic bulk velocity for the shocked wind material; however, any unsteady solution is bound to populate the nebula with magnetized turbulence, with a fast magnetosonic velocity close to c, which would lead to particle acceleration on a fast timescale, hence to efficient dissipation.

To summarize, both observational and theoretical arguments indicate that efficient dissipation of the magnetic field and the tapping of this energy into kinetic energy are relevant processes at the pulsar wind termination shock.

The last issue concerns the origin of radio-emitting electrons in the Crab nebula, which are about 10^2 more numerous than the optical to X-ray emitting electrons [58]. In terms of multiplicity, the radio emission suggests a pair multiplicity $\kappa \sim 10^6$, well above the theoretical expectations $\kappa \sim 10^2 - 10^4$ [73, 74], which are in much better agreement with the multiplicity associated to higher energy electrons. Two generic, diverging interpretations are usually given: either the multiplicity indeed reaches values $\kappa \sim 10^6$, in which case the pulsar spin-down power divided by the total kinetic energy leads to a rather low value

$\gamma_{\rm w} \lesssim 10^2 - 10^3$ for the Lorentz factor of the wind at the termination shock [69], or $\kappa \sim 10^4$ and, for one interpretation, the radio emitting low energy electrons were injected at an earlier stage of the nebula [18, 38, 45]. Interestingly, the latter interpretation requires that the Crab pulsar was born with a period of order $\sim 5\,$msec, i.e. quite close to the range of values that we are interested in [38].

Let us note that the present discussion implicitly assumes values $\kappa \ll 10^6$, as if κ were as high as 10^6, the ions could carry only a tiny fraction of the wind energy and it would become difficult to match the cosmic-ray flux at the highest energies; this issue is discussed in Sec. 3.

In spite of the above unknowns, the fact is that the Crab accelerates electron-positron pairs efficiently, up to the radiation reaction limit, with a high energy index very similar to that expected in a relativistic Fermi process, and this remains our main motivation to discuss the possibility of pushing ions to ultra-high energies. In what follows, we build a one-zone model of the synchrotron nebula in order to quantify the various losses that limit the acceleration of particles to ultra-high energies.

Following the above discussion, we assume that the wind energy is efficiently dissipated into random particle energies inside the nebula, i.e. $\sigma_{\rm PWN} \lesssim 1$; hereafter, $\sigma_{\rm PWN}$ is understood as the average magnetization parameter inside the nebula, after dissipation has taken place. This dissipation can either take place upstream of the termination shock, in which case the shock itself transforms the ordered kinetic energy into random particle energies; or, it can take place at or downstream of the termination shock, through one of the various processes discussed above. We also assume that the termination shock is strong, which implies super-fast magnetosonic velocities of the wind; this, however, is not a stringent requirement on wind physics, since it only requires a wind Lorentz factor at the termination shock $\gamma_{\rm w} \gtrsim \sigma_{\rm i}^{1/3} \sim \gamma_{\rm diss.}^{1/3} \sim 10^3$ for our fiducial parameters, see the definition of $\gamma_{\rm diss.}$ in Eq. (2.13) below, and $\sigma_{\rm i}$ corresponds to the initial magnetization of the wind [58].

2.2 The millisecond nebula structure

The structure of the nebula can be approximated by analytical solutions at times $t \lesssim t_{\rm sd}$, when $L_{\rm w}$ is approximately constant [75]. The pulsar wind nebula radius can then be written

$$R_{\rm PWN} = \left(\frac{125}{99}\frac{\beta_{\rm PWN}^3 c^3 L_0}{M_0}\right)^{1/5} t^{6/5} \qquad (t_{\rm c} \gtrsim t) \tag{2.3}$$

$$= \left(\frac{8}{15}\frac{L_0}{M_0}\right)^{1/2} t^{3/2} \qquad (t_{\rm sd} \gtrsim t \gtrsim t_{\rm c}) \ , \tag{2.4}$$

in terms of the time $t_{\rm c}$ at which the external shock of the PWN has swept up the mass of the supernova ejecta, M_0, which we assume of constant density (with a rapidly declining density profile beyond) and in terms of the wind power L_0; $\beta_{\rm PWN}$ represents the velocity of the pulsar wind nebula in the source rest frame. For parameters of interest, one finds that $t_{\rm sd} \gtrsim t_{\rm c}$, since $t_{\rm c} \sim 10^5\,{\rm s}\, L_{45}^{-1} M_{\rm ej,34} v_{\rm ej83}^2$ for a core mass $M_{\rm ej} = 5 M_{\rm ej,34} M_\odot$ and an ejecta velocity $v_{\rm ej} = 1000\, v_{\rm ej,8}\,{\rm km/s}$ [35, 75], hence we will use mostly Eq. (2.4) in the following.

At times $t \gtrsim t_{\rm sd}$, the pulsar input into the nebula decreases rapidly. For this phase, we then assume that the blast evolves in free expansion, meaning [35]

$$R_{\rm PWN}(t) = R_{\rm PWM}(t_{\rm sd}) \frac{t}{t_{\rm sd}} \tag{2.5}$$

Of course, we are mostly interested in the PWN structure at the time $t_{\rm sd}$, since it corresponds to the time of maximum energy injection into the nebula. The temporal scalings of $R_{\rm PWN}$ at times $t \ll t_{\rm sd}$ and $t \gg t_{\rm sd}$ thus do not play a crucial role in the forthcoming analysis, but they help in understanding how the various quantities evolve in time.

The above estimates neglect the interaction of the blast with the outer shocked region of the supernova, i.e. the forward and reverse shocks associated with the interaction with the circumstellar medium. In more typical, less powerful ($L_{\rm p} \lesssim 10^{39}\,{\rm erg/s}$) pulsar wind nebulae, the interaction with the reverse shock takes place on timescales of thousands of years and this leads to the compression of the nebula [50]. In the present case, the interaction takes place shortly after $t_{\rm c}$, i.e. shortly after the PWN external shock into the ejecta has swept up the inner core of the remnant. However, the pulsar energy output $E_{\rm rot} \sim 2\times10^{52}\,P_{-3}^2\,{\rm ergs}$ dominates the kinetic energy of the outer blast ($E_{\rm ej} \sim 10^{51}\,{\rm ergs}$), therefore the nebula will dominate the dynamics. We neglect this interaction phase; again, it should not modify appreciably the values of $R_{\rm PWN}$ that we derive at time $t_{\rm sd}$, which is our prime objective here.

The above analytical solutions also fail when radiative cooling of the blast becomes important. As we show in the following, the latter possiblity is to be considered, because the electrons cool through synchrotron faster than a dynamical timescale, contrary to what happens in PWNe such as the Crab. Therefore, if dissipation of the Poynting flux is efficient, and if ions represent a modest part of the energy budget, most of the wind luminosity input into the nebula is actually lost into radiation. In order to account for this effect, we use an improved version of Eqs. (2.3),(2.4), in which $L_0 = (1-\eta_{\rm rad})L_{\rm p}$ represents the actual power deposited into the nebula, $\eta_{\rm rad} = 1-\eta_B-\eta_{\rm i}$ representing the fraction of luminosity converted into radiation through pair cooling (η_B: fraction of energy in the magnetic field, $\eta_{\rm i}$: fraction of energy in ions, in the nebula). These approximations are used to provide analytical estimates of the various quantities characterizing the nebula at time $t_{\rm sd}$.

We complement these estimates with a detailed numerical integration of the following system:

$$\dot{R}_{\rm PWN} = \beta_{\rm PWN} c \tag{2.6}$$

$$\dot{R}_{\rm es} = \beta_{\rm es} c \tag{2.7}$$

$$\dot{U}_{\rm sw} = (\beta_{\rm w}-\beta_{\rm ts})\,L_{\rm w} - P_{\rm em} - 4\pi R_{\rm PWN}^2 \beta_{\rm PWN} c\, p_{\rm PWN}, \tag{2.8}$$

$$\dot{M}_{\rm se} = (\beta_{\rm es}-\beta_{\rm ej})\,4\pi r_{\rm es}^2 \rho_{\rm ej} c, \tag{2.9}$$

$$\dot{U}_{\rm se} = (\beta_{\rm es}-\beta_{\rm ej})\,4\pi r_{\rm es}^2 \rho_{\rm ej} c^3 + 4\pi R_{\rm PWN}^2 \beta_{\rm PWN} c\, p_{\rm PWN}. \tag{2.10}$$

All quantities are defined in the source rest frame; they are as follows: $R_{\rm PWN}$ corresponds to the radius of the contact discontinuity, interpreted as the size of the nebula; $R_{\rm es}$ represents the location of the outer shock of the nebula, propagating in the supernova remnant; to a very good approximation, $R_{\rm es} \simeq R_{\rm PWN}$ (thin-shell approximation); $\beta_{\rm es}$ consequently represents the velocity of this outer shock while $\beta_{\rm ts}$ denotes the velocity of the termination shock; $U_{\rm sw}$ represents the energy contained in the shocked wind region, beneath the contact discontinuity; $P_{\rm em}$ represents the power lost through radiation; since the electrons cool faster than an expansion timescale (see below), one can write $P_{\rm em} = (1-\eta_B-\eta_{\rm i})\,(\beta_{\rm w}-\beta_{\rm ts})\,L_{\rm w}$, in terms of the fraction of power injected into the nebula in magnetic field (η_B) and ions ($\eta_{\rm i}$). $p_{\rm PWN}$ represents the pressure inside the nebula, which can be well approximated by $U_{\rm sw}/(4\pi R_{\rm PWN}^3)$ [51]; the term associated to $p_{\rm PWN}$ consequently represents adiabatic losses for $U_{\rm sw}$; $M_{\rm se}$ denotes the mass accumulated in the shocked ejecta region, between the contact discontinuity and the outer shock; $\beta_{\rm ej}$ corresponds to the velocity of the supernova rem-

nant ejecta, in the source frame; finally, $U_{\rm se}$ denotes the energy contained in the shocked ejecta region. To a good approximation, $U_{\rm se} - M_{\rm se}c^2 \simeq M_{\rm se}\beta_{\rm PWN}^2 c^2/2$ since the ejecta is non-relativistic.

These equations can be obtained by integrating the equations of particle current density and energy-momentum conservation over the spatial variables, between the boundaries of interest. This procedure introduces the brackets $(\beta_{\rm w} - \beta_{\rm ts})$ for $\dot{U}_{\rm sw}$ and $(\beta_{\rm es} - \beta_{\rm ej})$ for $\dot{U}_{\rm se}$, which correspond to the fact that the boundaries of the shocked wind and shocked ejecta are delimited by the moving shock waves. The velocity of the termination shock in the source frame depends non-trivially on the degree of magnetization of the shock; for $\sigma \ll 1$, however, $\beta_{\rm ts} \ll \beta_{\rm w}$ [44] and $\beta_{\rm w} \simeq 1$, therefore we approximate $\beta_{\rm w} - \beta_{\rm ts} \simeq 1$. For the outer shock, assuming it is strong, non-radiative and non-relativistic, one has $\beta_{\rm es} - \beta_{\rm ej} \simeq 4(\beta_{\rm PWN} - \beta_{\rm ej})/3$. This closes the system.

In order to evaluate the dynamics of the nebula, we assume that the supernova ejecta consists of a core mass $5\,M_\odot$ of constant density. An analytical estimate of the size of the pulsar wind nebula $R_{\rm PWN}$ is then given by Eqs. (2.4) and (2.5):

$$\begin{aligned} R_{\rm PWN} &\simeq 4.1\times10^{16}\, L_{\rm p,45}^{1/2} t_{\rm sd,7.5}^{3/2} \check{t}^{3/2}\hat{t}\ {\rm cm} \\ &\simeq 3.2\times10^{16}\, P_{-3} B_{\star,13}^{-2} R_{\star,6}^{-6} I_{\star,45}^{3/2}\, \check{t}^{3/2}\hat{t}\ {\rm cm}\ . \end{aligned} \tag{2.11}$$

The quantities $\check{t} \equiv \min(1, t/t_{\rm sd})$ and $\hat{t} \equiv \max(1, t/t_{\rm sd})$ indicate the scaling of these values at times respectively short and long of $t_{\rm sd}$, obtained respectively through Eq. (2.4) and Eq. (2.5). Figure 1 presents the evolution in time of pulsar wind dynamical quantities ($R_{\rm PWN}$ and $B_{\rm PWN}$) calculated analytically and by numerical integration. The prefactors match the numerical evaluation shown in Fig. 1 for $\eta_{\rm rad} \lesssim 0.9$. The scaling departs slightly from the $t^{3/2}$ (resp. t) behaviour at short (resp. late) times compared to $t_{\rm sd}$, but we neglect this difference in the following. Radiative nebulae, in which $\eta_{\rm rad}$ is closer to unity, tend to be more compact; this difference can be read off Fig. 1 and inserted in the relations that follow. For the sake of simplicity, we assume an adiabatic case in the following, i.e. $1 - \eta_{\rm rad} \sim 1$.

At this stage, it may be useful to make contact with known pulsar wind nebulae, such as the Crab: its radius $R_{\rm PWN}$ is about 1 pc, i.e. about a hundred times larger than the above. In the Crab nebula, the radius of the termination shock is estimated to be $\sim 0.1\,{\rm pc}$ [44], while in the present case, the termination shock is located close to the contact discontinuity, see Sec. 2.4.1, making the above nebula not only more compact, but also much thinner.

The mean magnetic field in the nebula $B_{\rm PWN}$ is then obtained as follows. Recall that η_B corresponds to the magnetic fraction of the energy actually injected into the nebula after a proper account of dissipation, i.e. $\eta_B = \sigma_{\rm PWN}/(1+\sigma_{\rm PWN})$; one thus has

$$\begin{aligned} B_{\rm PWN} &= \left(\frac{6\eta_{\rm B}\int_0^t L_{\rm w}(t'){\rm d}t'}{R_{\rm PWN}^3}\right)^{1/2} \\ &\simeq 14\,\eta_{B,-1}^{1/2} L_{\rm p,45}^{-1/4} t_{\rm sd,7.5}^{-7/4} \check{t}^{-7/4}\hat{t}^{-3/2}\ {\rm G} \\ &\simeq 12\,P_{-3}^{-5/2}\eta_{B,-1}^{1/2} I_{\star,45}^{-7/4} B_{\star,13}^{3} R_{\star,6}^{9}\, \check{t}^{-7/4}\hat{t}^{-3/2}\ {\rm G}\ . \end{aligned} \tag{2.12}$$

The numerical values are obtained by plugging into the first equation the temporal scalings of $L_{\rm w}$ and $R_{\rm PWN}$ obtained previously. Analytical and numerical estimates agree for the adiabatic case at the spin-down time, see Fig. 1. The magnetic field strength is of course

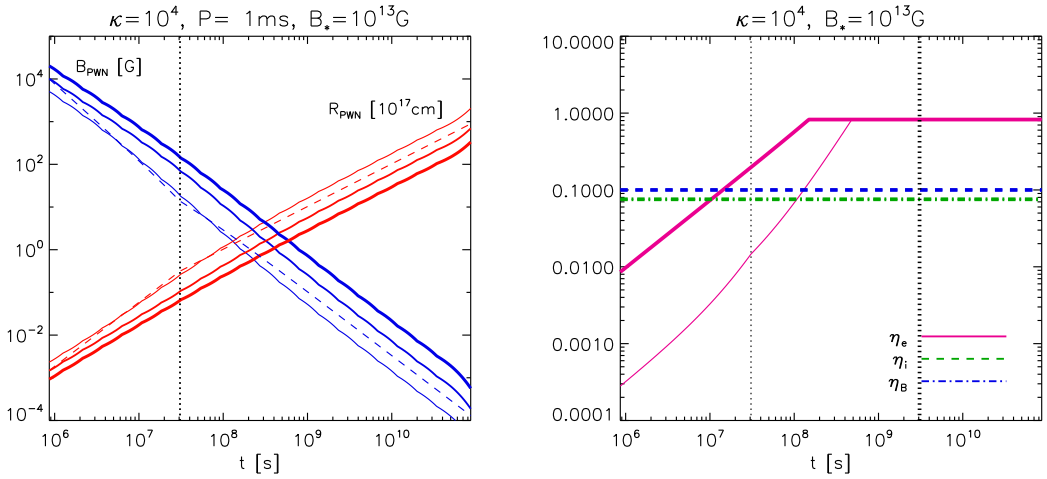

Figure 1. Evolution in time of pulsar wind dynamical quantities, for pulsar dipole magnetic field $B_{\star,13} = 1$, leptonic multiplicity $\kappa_4 = 1$ and assuming $\eta_{\rm B} = 0.1$. *Left:* Case of a pulsar with initial rotation period $P_{-3} = 1$. Red increasing lines: radius of the nebula (obtained by integrating numerically Eqs. 2.6−2.10). Increasing thickness for $\eta_{\rm rad} = 0, 0.9, 0.99$. The dashed lines represent the analytical adiabatic case (Eq. 2.11). Blue decreasing lines: corresponding mean magnetic field in the pulsar wind nebula $B_{\rm PWN}$ (Eq. 2.12). *Right:* Fraction of the pulsar luminosity dissipated into magnetic energy in the nebula (η_B, blue dashed), to leptons (η_e, pink solid) and to ions ($\eta_{\rm i}$, assuming protons, green dot-dashed). Initial rotation periods $P_{-3} = 1$ (thin lines), and $P_{-3} = 10$ (thick lines). The vertical dotted line indicates the spin-down timescale $t_{\rm sd}$.

much larger than that seen in more standard PWNe [50, 51, 76], as a result of the larger input energy and of the younger age, which implies a more compact nebula.

The right panel of Fig. 1 depicts the evolution of the distribution of the energy fractions $\eta_{\rm i}$, η_e and $\eta_{\rm B}$, discussed below.

2.3 Energy injected into particles in the nebula

As argued in Section 2.1, we assume efficient dissipation of the initial Poynting flux, into random particle energy. In the absence of energy losses, this conversion implies that particles (electron-positron pairs or ions) acquire a typical Lorentz factor

$$\begin{aligned}\gamma_{\rm diss.} &\simeq \frac{1}{1+\sigma_{\rm PWN}}\frac{L_{\rm w}}{\dot{N}mc^2} \\ &\simeq 2.2\times10^9\frac{1-\eta_{\rm B}}{1+x_{\rm i}}\kappa_4^{-1}L_{\rm p,45}^{1/2}\hat{t}^{-1} \\ &\simeq 1.8\times10^9\frac{1-\eta_{\rm B}}{1+x_{\rm i}}\kappa_4^{-1}P_{-3}^{-2}B_{\star,13}R_{\star,6}^3\hat{t}^{-1}\ . \end{aligned} \tag{2.13}$$

This Lorentz factor $\gamma_{\rm diss.}$ can also be written as: $\gamma_{\rm diss.} = \gamma_{\rm w}(1+\sigma_{\rm ts})/(1+\sigma_{\rm PWN})$ in terms of $\sigma_{\rm ts}$, the magnetization of the flow short of the termination shock. The particle rest mass power injected into the nebula is written here: $\dot{N}mc^2 \equiv 2\kappa\,\dot{N}_{\rm GJ}m_ec^2(1+x_i)$, with $\dot{N}_{\rm GJ} = e^{-1}\sqrt{L_{\rm w}c}$ the Goldreich-Julian rate [77]; $x_{\rm i}$ is the ratio of the power injected into ions, relatively to that injected into pairs: if ions of charge $Z_{\rm i}$ are injected at a rate $\dot{N}_{\rm GJ}/Z_{\rm i}$, $x_{\rm i} \equiv m_{\rm i}/(2Z_{\rm i}\kappa m_e)$, so that $x_{\rm i} \lesssim 1$ for $\kappa \gtrsim 10^3$.

Up to radiation reaction effects, heating through dissipation proceeds equally for pairs and ions, meaning that both acquire a same Lorentz factor. This is guaranteed for all dissipation processes mentioned earlier. Among others, this implies that, notwithstanding radiation reaction effects, the ratio of the energy injected into pairs to that injected into ions is conserved in the dissipative processes.

At the present time, one cannot predict what kind of ions the pulsar would output. We therefore remain general and consider ions of mass number $A_{\rm i}$, charge $Z_{\rm i}$. Note that the composition of the highest energy cosmic rays is not very well-known either: while the Pierre Auger Collaboration reports a light composition at $10^{19}\,{\rm eV}$, transiting to an intermediate composition at higher energies [78], the results of the Telescope Array experiment seemingly point towards a light composition [79], even though the depths of shower maximum of both experiments appear compatible, see [80].

Actually, energy losses may limit the typical Lorentz factor γ_e of electron-positron pairs to the minimum of $\gamma_{\rm diss.}$ and the radiation reaction limiting Lorentz factor $\gamma_{\rm e-loss}$. Of course, γ_e cannot be lower than the Lorentz factor of the wind at the termination shock, $\gamma_{\rm w}$, which is unknown. We assume that $\gamma_{\rm w} < \min\left(\gamma_{\rm diss.},\gamma_{\rm e-loss}\right)$. This is not a strong assumption, since the latter two Lorentz factors are quite large.

Equating the synchrotron cooling time with the gyration time of the particle, the radiation reaction limiting Lorentz factor $\gamma_{\rm e-loss}$ is given by the usual formula

$$\begin{aligned}\gamma_{\rm e-loss} &= \frac{3}{2}\frac{m_e c^2}{e^{3/2}B_{\rm PWN}^{1/2}}\\ &\simeq 3\times10^7\eta_{B,-1}^{-1/4}L_{\rm p,45}^{1/8}t_{\rm sd,7.5}^{7/8}\check{t}^{7/8}\hat{t}^{9/8}\\ &\simeq 3\times10^7\,\eta_{B,-1}^{-1/4}P_{-3}^{5/4}I_{\star,45}^{7/8}B_{\star,13}^{-3/2}R_{\star,6}^{-9/2}\check{t}^{7/8}\hat{t}^{9/8}\ .\end{aligned}\tag{2.14}$$

The synchrotron power of ions of Lorentz factor γ, atomic number Z_i and mass number A_i scales as $P_{\rm syn} = (Z_{\rm i}^4/A_{\rm i}^2)(m_e/m_p)^2(4/3)\sigma_{\rm T}U_B c\gamma^2\beta^2$, therefore the radiation reaction Lorentz factor for ions is a factor $A_{\rm i}Z_{\rm i}^{-3/2}m_p/m_e$ larger than $\gamma_{\rm e-loss}$. For ions, radiation reaction therefore does not limit the efficiency of dissipation.

Accounting for dissipation and radiation reaction limitations, one can thus write the fractions of energy η_e and η_i carried by the electrons and the ions inside the nebula as:

$$\eta_e = \frac{1-\eta_B}{1+x_{\rm i}}\min\left(1,\frac{\gamma_{\rm e-loss}}{\gamma_{\rm diss.}}\right)\ ,\quad \eta_i = \frac{(1-\eta_B)x_{\rm i}}{1+x_{\rm i}}\ .\tag{2.15}$$

The quantity η_e is understood as characterizing the energy injected in pairs in the nebula, after dissipation/acceleration processes, but before synchrotron cooling has taken place. Clearly, for the above fiducial parameters, $\eta_e \ll 1$ at time $t_{\rm sd}$, meaning that most of the energy dissipated into the electrons has been radiated at the radiation reaction limit, producing photons of energy $\sim 50\,{\rm MeV}$. This radiation does not contribute to the radiation losses of ultra-high energy ions but it may lead to a specific signature of dissipation processes in such young PWNe. In contrast, $\gamma_{\rm e-loss} \gg \gamma_{\rm diss.}$ in the Crab nebula, so that the electrons can take away most of the dissipated energy without losing it to radiation.

In such compact PWNe, the electrons cool through synchrotron radiation on a timescale that is much shorter than a dynamical timescale, down to non-relativistic velocities, since

the cooling Lorentz factor is given by

$$\begin{aligned}\gamma_{\rm c} &\simeq \frac{6\pi m_e c^2 \beta_{\rm PWN}}{\sigma_{\rm T} B_{\rm PWN}^2 R_{\rm PWN}} \\ &\sim t_{\rm sd,7.5}^2 \beta_{\rm PWN} \eta_{B,-1}^{-1} \check{t}^2 \hat{t}^2 \\ &\sim \eta_{B,-1}^{-1} P_{-3}^4 \beta_{\rm PWN} B_{\star,13}^{-4} R_{\star,6}^{-12} I_{45}^2 \check{t}^2 \hat{t}^2 \ . \end{aligned} \tag{2.16}$$

This represents a major difference with respect to the case of the Crab nebula, for which $\gamma_{\rm c} \gg 1$, so that most electrons do not cool on an expansion timescale, due to the smaller amount of energy injected into the wind and to the larger size of the nebula.

The above allows us to characterize the spectral energy distribution (SED) of the nebula; in particular, the low-frequency spectral luminosity is represented by

$$L_{\nu,{\rm syn}} \simeq \eta_e L_{\rm w} \left(\frac{\epsilon}{\epsilon_e}\right)^{1/2} \qquad (\epsilon_{\rm c} < \epsilon < \epsilon_e) \tag{2.17}$$

with $\epsilon_{\rm c} = h\nu_{\rm c}$ and $\epsilon_e = h\nu_{\rm e}$ in terms of the synchrotron peak frequencies associated to Lorentz factors $\gamma_{\rm c}$ and $\gamma_e = \min(\gamma_{\rm e-loss}, \gamma_{\rm diss.})$. In Fig. 1, we plot the time evolution of the various quantities that characterize the nebula, i.e. the mean magnetic field, the mean nebular radius and the fractions of energy η_e, η_B and $\eta_{\rm i}$.

2.4 Ion acceleration

After their injection through the termination shock, the ions are energized through dissipative processes up to $\gamma_{\rm diss.}$, then shock accelerated to the maximal Lorentz factor $\gamma_{\rm max}$ that we seek to determine here. This latter Lorentz factor is given, as usual, by the competition between shock acceleration, escape from the PWN and energy losses in the synchrotron nebula.

We assume here that acceleration proceeds at the Bohm rate, an assumption that is motivated and supported by the two following remarks. The first is of a more empirical nature as it follows from the observation that the Crab nebula does accelerate electron-positron pairs up to the radiation reaction limit. If the acceleration timescale is written $t_{\rm acc} = \mathcal{A} t_{\rm g}$, then the comparison of $t_{\rm acc}$ with the synchrotron loss timescales leads to an upper bound on the maximum photon energy, $\epsilon_\gamma \lesssim \mathcal{A}^{-1}\, m_e c^2/\alpha_{\rm em}$. The fact that the synchrotron spectrum extends up to $\sim 60\,{\rm MeV}$ or so in the Crab nebula indicates that $\mathcal{A} \sim 1$.

The second line of argument originates from our theoretical understanding of particle acceleration at relativistic shock waves; to put it briefly, $\mathcal{A} \sim 1$ if some large scale turbulence, seeded downstream of the termination shock by dissipative processes, mediates the scattering process at the termination shock. In order to see this, one must recall that supra-thermal particles probe a short length scale of order $\sim r_{\rm g}$ behind a relativistic oblique shock, before returning to the shock or being advected away [62]. Therefore, if some turbulence is transmitted from upstream to downstream through the shock, the shock crossing conditions imply the continuity of the magnetic field lines through the shock, which then prevent repeated Fermi cycles, unless most of the turbulent power lie on short length scales [60, 62, 64, 81]. If, however, the turbulence is seeded downstream of the shock, which requires additional dissipative processes as in the present case, then this continuity is broken, hence Fermi cycles can take place, as modelled in test-particle Monte Carlo simulations, e.g. [19–22]. The downstream and upstream residence timescales are then both of order $r_{\rm g}$ in the shock rest frame, so that the acceleration timescale corresponds to $\mathcal{A} \sim \mathcal{O}(1)$.

2.4.1 Confinement at the shock and in the nebula

Confinement in the nebula itself leads to a maximal Lorentz factor:

$$\begin{aligned}\gamma_{\rm conf} &\sim \frac{Z_{\rm i} e B_{\rm PWN} R_{\rm PWN}}{m_{\rm i} c^2} \\ &\simeq 1.5\times10^{11}\,\frac{Z_{\rm i}}{A_{\rm i}}\,\eta_{B,-1}^{1/2} L_{\rm p,45}^{1/4} t_{\rm sd,7.5}^{-1/4} \check{t}^{-1/4} \hat{t}^{-1/2} \qquad (2.18)\\ &\simeq 1.4\times10^{11}\,\frac{Z_{\rm i}}{A_{\rm i}}\,\eta_{B,-1}^{1/2} P_{-3}^{-3/2} I_{\star,45}^{-1/4} B_{\star,13} R_{\star,6}^{3} \check{t}^{-1/4} \hat{t}^{-1/2}\ . \qquad (2.19)\end{aligned}$$

The large value of $\gamma_{\rm conf}$ confirms that young fast pulsars input enough power into the nebula to confine particles up to ultra-high energies, a non-trivial result in itself.

As a matter of fact, the finite size of the termination shock limits the maximum acceleration energy to a factor ~ 2 below the above confinement energy, because the shock radius $r_{\rm ts} \sim \alpha_{\rm ts} R_{\rm PWN}$ with $\alpha_{\rm ts} \sim 0.4$. This value is derived from the numerical simulations discussed in Sec. 2.2, but it can be understood as follows. In the source rest frame, one can write the velocity of the termination shock to first order in $1/\gamma_{\rm w}$ as follows,

$$\beta_{\rm ts} \simeq \frac{1-3\beta_2}{-3+\beta_2} \qquad (2.20)$$

where β_2 denotes the velocity of the shocked wind, immediately downstream of the termination shock. This equation assumes hydrodynamic jump conditions at the shock to simplify the analysis. It is essentially a rewriting of the shock velocity in a frame in which the downstream is moving at velocity $\beta_{\rm PWN}$; the expression in the downstream frame is obtained by $\beta_2 \to 0$, which implies $\beta_{\rm ts} \to -1/3$, as expected for a strong ultra-relativistic hydrodynamic shock wave [82]. One commonly assumes that the flow velocity then evolves as a function of radius according to $\beta \propto r^{-2}$, see [44, 45] for a detailed discussion; this implies that the blast velocity $\beta_{\rm PWN} \simeq \beta_2 (R_{\rm PWN}/r_{\rm ts})^2$. Since $R_{\rm PWN}/r_{\rm ts} \simeq \beta_{\rm PWN}/\beta_{\rm ts}$, one can solve $r_{\rm ts}/R_{\rm PWN}$ as a function of $\beta_{\rm PWN}$, using the above in conjunction with Eq. (2.20). One finds

$$r_{\rm ts} \simeq \left[\sqrt{3\beta_{\rm b}} + \mathcal{O}(\beta_{\rm PWN}^2)\right] R_{\rm PWN}\ . \qquad (2.21)$$

Therefore, $\alpha_{\rm ts} \simeq \sqrt{3\beta_{\rm PWN}} \sim 0.4$ for a typical velocity $\beta_{\rm PWN} \sim 0.05$ at $t_{\rm sd}$ (a value checked in numerical calculations).

At a gyroradius $r_{\rm g}$ a factor of order unity to a few above $r_{\rm ts}$, the particle feels the shock curvature and it gradually decouples from the flow as its size exceeds the size of the accelerator. Acceleration therefore stops at Lorentz factor

$$\gamma_{\rm max} \simeq \alpha_{\rm ts}\gamma_{\rm conf} \qquad (2.22)$$

2.4.2 Synchrotron losses

Due to the strong magnetic field in the nebula, synchrotron losses represent a potential limitation to the maximum energy. In the course of acceleration, synchrotron losses limit γ to

$$\begin{aligned}\gamma_{\rm i,syn-acc} &\simeq 6.2\times10^{10}\eta_{B,-1}^{-1/4} A_{\rm i} Z_{\rm i}^{-3/2} L_{45}^{1/8} t_{\rm sd,7.5}^{7/8} \check{t}^{7/8} \hat{t}^{3/4} \\ &\simeq 6.0\times10^{10}\eta_{B,-1}^{-1/4} A_{\rm i} Z_{\rm i}^{-3/2} P_{-3}^{5/4} B_{\star,13}^{-3/2} R_{\star,6}^{-9/2} I_{\star,45}^{7/8} \check{t}^{7/8} \hat{t}^{3/4} \qquad (2.23)\end{aligned}$$

As discussed in Sec. 2.3, this maximum Lorentz factor is simply γ_e times $A_{\rm i} Z_{\rm i}^{-3/2} m_p/m_e$. It lies a factor of a few below the confinement energy, but it nevertheless allows protons to be accelerated up to energies of the order of the GZK cut-off for our fiducial parameters.

Given that $r_{\rm ts} \lesssim R_{\rm PWN}$, particles also suffer synchrotron energy losses during their escape out of the nebula. The corresponding cooling Lorentz factor is obtained by matching $P_{\rm syn} R_{\rm PWN}/c$ and the particle energy, which leads to

$$\begin{aligned}\gamma_{\rm i,syn-esc} &\simeq 2.6\times10^{10}\,\eta_{B,-1}^{-1} A_{\rm i}^3 Z_{\rm i}^{-4} t_{\rm sd,7.5}^2 \check{t}^2 \hat{t}^2 \\ &\simeq 2.4\times10^{10}\,\eta_{B,-1}^{-1} A_{\rm i}^3 Z_{\rm i}^{-4} P_{-3}^4 B_{\star,13}^{-4} R_{\star,6}^{-12} I_{\star,45}^2 \check{t}^2 \hat{t}^2 \end{aligned} \tag{2.24}$$

As a result of its combination of powers of $t_{\rm sd}$, $\hat{t}$ and $\check{t}$, the above equation can actually be rewritten as $\gamma_{\rm i,syn-esc} \simeq 2.5\times10^{10}\,\eta_{B,-1}^{-1} A_{\rm i}^3 Z_{\rm i}^{-4}\,(t/1\,{\rm yr})^2$, with a numerical prefactor entirely controlled by the core mass of the supernova ejecta and by fundamental constants. However, we are interested in computing the limiting Lorentz factor at a time $t_{\rm sd}$, at which most of the rotational energy has been output by the pulsar; for this reason, one should actually read Eq. (2.24) above with $\hat{t} = \check{t} = 1$, which *de facto* introduces a dependence on $t_{\rm sd}^2$.

This limit appears more severe than the previous ones, but with a rather strong dependance on the spin-down time $t_{\rm sd}$, or alternatively, on the dipole moment $\mu = B_\star R_\star^3/2$ of the neutron star, see Eq. (2.2). Therefore, a spin-down time larger by a factor two, or a (modest) factor $\sqrt{2}$ decrease in μ would push this maximum energy [as well as Eq. (2.23)] at or above $10^{20}\,$eV for protons, while the maximal energy associated to the finite size of the termination shock at $\hat{t} = \check{t} = 1$ would remain of the order to $10^{20}\,$eV. Note that the total injected energy $E \sim E_{\rm rot} \simeq L_{\rm w} t_{\rm sd}$ does not depend on μ. Alternatively, if one assumes $\eta_B \sim 1$, a magnetic field $B_\star \sim 3\times10^{12}\,$G would still guarantee that the limiting synchrotron loss energy lies above the GZK energy (for protons), just as the maximum energy associated to the finite size of the termination shock.

Of course, synchrotron energy losses are much weaker for ions with $A_{\rm i} > 1$; the corresponding maximal energy is larger than that of protons by a factor $(A_{\rm i}/Z_{\rm i})^4 \sim 16$.

2.4.3 Photohadronic losses

Assuming that the injected ions are protons, the impact of photopion interactions can be evaluated in the standard $\Delta-$approximation, according to which interactions take place with photons of energy $\epsilon_{\gamma\pi} \sim 0.3\,{\rm GeV}/\gamma_{\rm p}$, with $\gamma_{\rm p}$ the proton Lorentz factor and cross-section $\sigma_{\gamma\pi} \sim 0.5\,$mb. It is straightforward to check that all protons interact with photons in the low-frequency part $\lesssim \nu_e$ of the synchrotron SED, which justifies our neglect of the high-frequency part of the synchrotron SED. The number density of such low-frequency synchrotron photons is[3]

$$\epsilon_\gamma \frac{{\rm d}n_\gamma}{{\rm d}\epsilon_\gamma} \simeq \eta_e \left(\frac{\epsilon_\gamma}{\epsilon_e}\right)^{1/2} \frac{L_{\rm w}}{4\pi R_{\rm PWN}^2 c \epsilon_\gamma} \quad (\epsilon_{\rm c} < \epsilon_\gamma < \epsilon_e) \tag{2.25}$$

so that the pion production optical depth, $\tau_{\gamma\pi} = R_{\rm PWN}\sigma_{\gamma\pi}\epsilon_\gamma {\rm d}n_\gamma/{\rm d}\epsilon_\gamma$ reads:

$$\begin{aligned}\tau_{\gamma\pi} &\simeq 7.9\times10^{-3}\,\eta_e\,\gamma_{\rm p,11}^{1/2} L_{\rm p,45}^{1/2} t_{\rm sd,7.5}^{-3/2} \check{t}^{-3/2} \hat{t}^{-3} \\ &\simeq 6.6\times10^{-3}\,\eta_e\,\gamma_{\rm p,11}^{1/2} P_{-3}^{-5} B_{\star,13}^4 R_{\star,6}^{12} I_{\star,45}^{-3/2} \check{t}^{-3/2} \hat{t}^{-3}\ , \end{aligned} \tag{2.26}$$

with $\gamma_{\rm p,11} = \gamma_{\rm p}/10^{11}$. Note that η_e depends on time, in particular $\eta_e \ll 1$ at early times, see Eq. (2.15) and Fig. 1, while $\eta_e \sim 1$ at late times.

[3] for clarity, we assume $1 + x_{\rm i} \sim 1$, $1 - \eta_B \sim 1$ in the expressions that follow

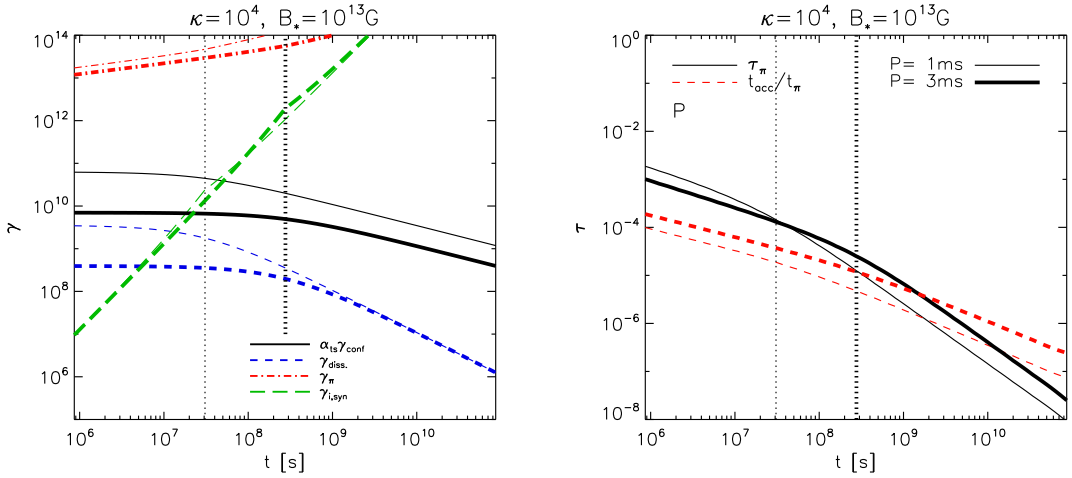

Figure 2. *Left:* Comparison of maximum Lorentz factors for proton confinement ($\gamma_{\rm conf}$, solid lines), acceleration ($\gamma_{\rm diss.}$, dashed lines) and energy loss by pion production (γ_π, red dot-dashed lines) and by synchrotron cooling ($\gamma_{\rm i,syn}$, green long-dashed lines), for pulsar initial rotation period $P_{-3} = 1, 3$ (increasing thickness), dipole magnetic field $B_{\star,13} = 1$, leptonic multiplicity $\kappa_4 = 1$, $\eta_{\rm rad} = 0$ and $\eta_{\rm B} = 0.1$. The vertical dotted line indicates the spin-down timescale $t_{\rm sd}$ corresponding to each rotation period (increasing thickness). See the text for details, in particular regarding the dependence of these curves on the parameters of the neutron star. *Right:* Corresponding pion production optical depth (black solid) and ratio of the acceleration timescale, $t_{\rm acc}$, to the pion production timescale, $t_{\gamma\pi}$, (red dashed) for a proton at Lorentz factor 10^{11}.

The ratio of the acceleration timescale to pion production timescale,

$$\frac{t_{\rm acc}}{t_{\gamma\pi}} \simeq \frac{\gamma_p}{\gamma_{\rm conf}} \tau_{\gamma\pi} \ , \tag{2.27}$$

indicates that pion production is not a limiting factor for acceleration to the highest energies.

The left panel of figure 2 presents the time evolution of the proton confinement Lorentz factor $\gamma_{\rm conf}$, dissipation Lorentz factors $\gamma_{\rm diss.}$, and limiting Lorentz factor from synchrotron losses $\gamma_{\rm i,syn}$ and pion production interactions γ_π, for initial periods $P = 1, 3, 10\,$ms.

The evolution over time of the pion production optical depth and the ratio of the acceleration to pion production timescales, calculated at the at energy $\gamma_{\rm p,11}$ are shown in the right panel of Fig. 2.

The same type of calculations can be performed for heavier nuclei, considering the Giant Dipole Resonance (GDR) as the main channel for energy losses on the background photons. The parameters for such interactions read: $\sigma_{A\gamma} \sim 8 \times 10^{-26}\, A_{56}\,{\rm cm}^{-2}$ for the cross-section, and $\epsilon_{\rm GDR} \sim 18\, A_{56}^{-0.21}\,{\rm MeV}/\gamma_{\rm i}$ [83]. The results for iron nuclei are presented in Fig. 3.

All in all, Equations (2.22), (2.23), (2.24) and (2.27) and the accompanying discussion thus indicate that proton (and heavier ion) acceleration to energies of the order of or above the GZK cut-off appears possible in PWNe with parameters close to those chosen in this paper, namely $B_{\star,13} \sim 1$, $P_{-3} \sim 1\,$ms, $\eta_B \sim 0.1 - 1$.

3 Discussion

Equations 2.19, (2.23), (2.24), 2.26 and 2.27 summarize the confinement and acceleration properties of young powerful pulsar wind nebulae at time $t_{\rm sd}$, when most of the rotational

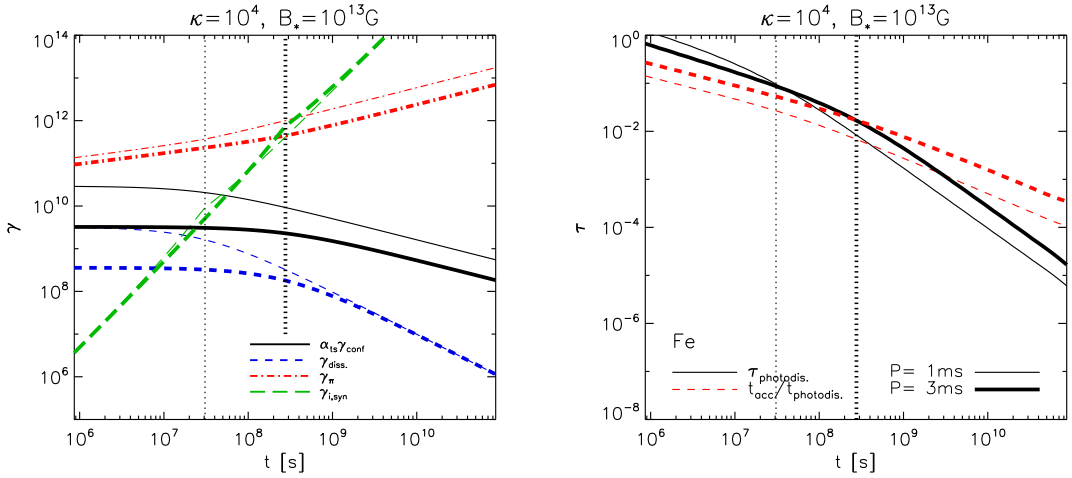

Figure 3. Same as Fig. 2, but for iron nuclei.

energy is output into the nebula. A third constraint on potential ultra-high energy cosmic ray sources comes from the energy output into cosmic rays above $10^{19}\,$eV. For a proton dominated composition, this energy output must match $\dot{\epsilon} \simeq 0.5 \times 10^{44}\,$ergs/Mpc^3/yr once it is folded over the population of sources with ocurrence rate $\dot{n}$ [6].

Over $t_{\rm sd}$, the pulsar injects into ions

$$E_{\rm i} \,=\, \eta_{\rm i}\, L_{\rm w}\, t_{\rm sd} \,=\, \frac{(1-\eta_B) x_{\rm i}}{(1+x_{\rm i})} L_{\rm p} t_{\rm sd}\ . \tag{3.1}$$

Assuming that these msec PWNe constitute a fraction $\eta_{\rm SN}$ of the total core collapse supernovae, with ocurrence rate $\dot{n}_{\rm SN} \sim 5 \times 10^{-5}\,$Mpc^{-3}yr^{-1}, the normalization to the flux of ultra-high energy cosmic rays thus implies

$$\eta_{\rm SN} \,\sim\, 3 \times 10^{-5} q_{\rm i}\, x_{\rm i}^{-1}\, L_{\rm p,45}^{-1} t_{\rm sd,7.5}^{-1}\ , \tag{3.2}$$

assuming here $x_{\rm i} \lesssim 1$, i.e. $\kappa \gtrsim 10^3$, and $1-\eta_{\rm B} \sim 1$. Recall that $x_{\rm i} \simeq 0.09 (A_{\rm i}/Z_{\rm i}) \kappa_4^{-1}$, indicating that these young msec pulsars should constitute a fraction $\sim 0.03\%$ of the supernova rate. If one rather wishes to normalize the flux at an energy $10^{18}\,$eV with $s \sim 2$, then this fraction would go up to $\sim 1\%$. The prefactor $q_{\rm i} \equiv (s-2)/\left\{1-[\gamma_{\rm max}(t_{\rm sd})/\gamma_{\rm diss.}(t_{\rm sd})]^{2-s}\right\}$ for an injection spectral index s, accounts for the difference in normalization induced by the lower cosmic-ray injection energy limit.

3.1 Neutrino signal for a proton-dominated composition

The detection of neutrinos associated with hadronic and photo-hadronic interactions of nuclei in the nebula would provide an unambiguous test of the present scenario. Let us first consider the yield of neutrinos through photo-hadronic interactions on the nebula SED. Since the neutrino yield for heavy nuclei is much smaller than that for protons, we assume in this section that $Z_{\rm i} = A_{\rm i} = 1$. The neutrino spectrum is then shaped by the accelerated proton spectrum and by the conversion efficiency. A parent proton produces 3 neutrinos per $p-n$ conversion, which takes place with probability 1/3 in each photopion interaction, thus on a timescale $t_{\gamma\pi^+} = 3 t_{\gamma\pi}$. At the detector, the neutrino carries a fraction $f_\nu/(1+z) \simeq 0.05/(1+z)$ of the parent proton energy, i.e. $E_\nu \simeq f_\nu E_{\rm i}/(1+z)$, with z the redshift of the source.

The time-dependent neutrino spectrum emitted by one PWN at luminosity distance $D_{\rm L}$ can be written:

$$E_\nu^2 \Phi_\nu(E_\nu, t) \;=\; \frac{(1+z)}{4\pi D_{\rm L}^2} E_\nu^2 \frac{3}{t_{\gamma\pi^+}(E_{\rm i})} \frac{{\rm d}E_{\rm i}}{{\rm d}E_\nu} \frac{{\rm d}N_{\rm i}}{{\rm d}E_{\rm i}} \;, \tag{3.3}$$

in terms of the parent proton spectrum ${\rm d}N_{\rm i}/{\rm d}E_i$ in the source. The latter is formally given by

$$\frac{{\rm d}N_{\rm i}(t)}{{\rm d}E_{\rm i}} \;=\; \eta_{\rm i} \int_0^t q_{\rm i}(t') \frac{L_{\rm w}(t')}{E_{\rm diss.}^2} \left[\frac{E_{\rm i,0}(t')}{E_{\rm diss.}(t')}\right]^{-s} \frac{{\rm d}E_{\rm i,0}(t')}{{\rm d}E_{\rm i}} \, e^{-\int_{t'}^t {\rm d}t''/t_{\rm exit}[t'', E_{i,0}(t'')]} \, {\rm d}t' \;, \tag{3.4}$$

with $q_{\rm i}(t') \;=\; (s-2)/\left\{1 - [\gamma_{\rm max}(t')/\gamma_{\rm diss.}(t')]^{2-s}\right\}$ a normalization prefactor. The energy $E_{\rm diss.} \equiv \gamma_{\rm diss.} m_p c^2$, while $E_{\rm i,0}(t')$ represents the energy of the proton at time t', which shifts down to $E_{\rm i}$ at time t due to adiabatic losses. The timescale $t_{\rm exit} \;=\; \left(t_{\gamma\pi^+}^{-1} + t_{\rm esc}^{-1}\right)^{-1}$ represents the timescale on which protons leave the source, either through $p-n$ conversion or through direct escape on timescale $t_{\rm esc}$. This solution neglects the energy loss associated with photo-pion production; the latter is small and the probability of exiting directly the source as a neutron significant, therefore photo-pion production effectively acts as a loss term from the nebula.

In order to simplify the above calculation, we make the usual approximation, e.g. [84], that neutrino production takes place during a timescale $t_{\rm loss} \;=\; \left[t_{\rm ad}^{-1} + t_{\rm esc}^{-1} + t_{\gamma\pi+}^{-1}\right]^{-1}$ and that the proton spectrum can be described by its time average on that timescale. Here, $t_{\rm ad} \;=\; R_{\rm PWN}/(\beta_{\rm PWN} c)$ characterizes the adiabatic loss timescale. Direct escape takes place on timescale $t_{\rm esc} \;\simeq\; R_{\rm PWN}\,(\gamma_{\rm i}/\gamma_{\rm conf})^{-1}$, corresponding to the assumption of diffusive escape with a Bohm scattering timescale $\sim r_{\rm g}/c$. The average proton spectrum is

$$\left\langle \frac{{\rm d}N_{\rm i}(t)}{{\rm d}E_{\rm i}} \right\rangle \;=\; \min\left(1, \frac{t_{\rm loss}}{t_{\rm sd}}\right) \frac{\eta_i q_i L_{\rm p} t_{\rm sd}}{E_{\rm diss.}^2} \left(\frac{E_{\rm i}}{E_{\rm diss.}^2}\right)^{-s} \;. \tag{3.5}$$

Indeed, if $t_{\rm loss} \;\gg\; t_{\rm sd}$, the pulsar luminosity function can be approximated as impulsive, $L_{\rm w} \;\sim\; t_{\rm sd} L_{\rm p} \delta(t - t_{\rm sd})$, while if $t_{\rm loss} \;\ll\; t_{\rm sd}$, the luminosity is approximately constant up to time $t_{\rm sd}$, but at any time, the energy contained in protons is a fraction $t_{\rm loss}/t_{\rm sd}$ of the energy injected over time $t_{\rm sd}$. One thus derives a neutrino energy flux

$$E_\nu^2 \Phi_\nu \;\simeq\; \frac{1+z}{4\pi D_{\rm L}^2} \frac{f_\nu}{t_{\gamma\pi}} \min\left(1, \frac{t_{\rm loss}}{t_{\rm sd}}\right) \eta_{\rm i} q_{\rm i} L_{\rm p} t_{\rm sd} \left(\frac{E_\nu}{E_{\nu\star}^2}\right)^{2-s} \;, \tag{3.6}$$

with $E_{\nu\star} \;\equiv\; f_\nu E_{\rm diss.}/(1+z)$.

The diffuse neutrino flux produced by such PWNe can be evaluated as follows. Writing $\dot{n}_{\rm s}$ the ocurrence rate per comoving volume element, the effective density at any time is $\max\left(t_{\rm loss}, t_{\rm sd}\right) \dot{n}_{\rm s}$, since $\max\left(t_{\rm loss}, t_{\rm sd}\right)$ indicates the effective duration of neutrino emission. The diffuse energy flux then reads

$$E_\nu^2 j_\nu \;=\; \frac{c}{4\pi} \int_0^{+\infty} \frac{{\rm d}z}{H(z)(1+z)} \dot{n}_{\rm s} \frac{t_{\rm loss}}{t_{\gamma\pi}} f_\nu \, \eta_{\rm i} q_{\rm i} L_{\rm p} t_{\rm sd} \left(\frac{E_\nu}{E_{\nu\star}^2}\right)^{2-s} \;. \tag{3.7}$$

Note that $\dot{n}_{\rm s}$ may contain a redshift dependence, and that $t_{\rm loss}$ and $t_{\gamma\pi}$ depend on the (source rest-frame) energy $(1+z)E_\nu$.

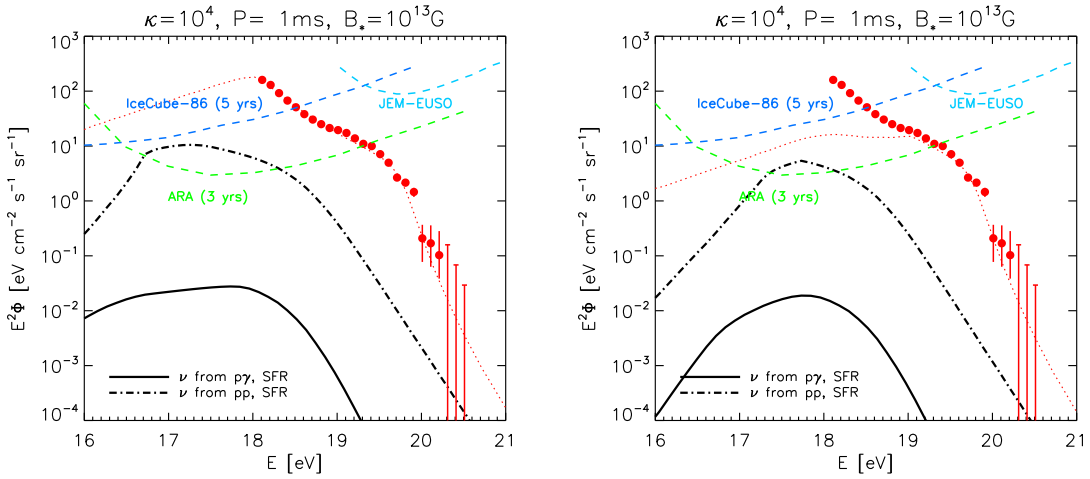

Figure 4. Neutrino spectra produced via pp (dot-dashed) and $p\gamma$ (solid) interactions for a population of pulsars with initial rotation period $P_{-3} = 1$, dipole magnetic field $B_{\star,13} = 1$, leptonic multiplicity $\kappa_4 = 1$, $\eta_{\rm rad} = 0$, $\eta_{\rm B} = 0.1$; left panel: cosmic ray flux normalized to the data at $> 10^{18}\,$eV; right panel: cosmic ray flux normalized to the data at $> 10^{19}\,$eV . The sensitivity of IceCube-86 for 5 years [85], JEM-EUSO [86], and ARA-37 for 3 years [87] are overplotted. In red dotted lines, the fit to the UHECR spectrum measured by the Auger Observatory [88], in red circles.

In order to evaluate the neutrino flux that results from pp interactions in the nebula environment, we consider only the interactions that arise as the cosmic rays cross the supernova remnant, given the very low density of particles within the nebula itself. As discussed in Ref. [30], the optical depth to pp interactions during the crossing of a $10 M_\odot$ supernova remnant can be written

$$\tau_{pp} \simeq \frac{0.3\,{\rm yr}}{t_{\rm esc}} \,. \tag{3.8}$$

The pp interactions only take place whenever $t_{\rm esc} < t_{\rm ad}$ and $t_{\rm esc} < t_{\gamma\pi^+}$. Given the small optical depth to photo-pion production, the latter condition is always satisfied; the former amounts to $\gamma > \beta_{\rm PWN}\gamma_{\rm conf}$, therefore the pp neutrino signal only concerns the highest energy range. It is then straightforward to evaluate the diffuse pp neutrino flux from Eq. (3.7), making the substitution $t_{\rm loss}/t_{\gamma\pi} \to \min(\tau_{pp}, 1) c t_{\rm esc}/R_{\rm PWN}$.

Figure 4 presents the neutrino spectrum produced by protons accelerated with a spectral index of $s = 2.2$, for a population of pulsars with identical parameters, with initial rotation period $P_{-3} = 1$, dipole magnetic field $B_{\star,13} = 1$, leptonic multiplicity $\kappa_4 = 1$, $\eta_{\rm rad} = 0$, $\eta_{\rm B} = 0.1$. The birth rate of these sources are assumed to have an occurrence rate scaled to the star formation rate (SFR) with $\dot{n}_{\rm s} = 800\,{\rm Gpc^{-3}\,yr^{-1}}$ at $z = 0$ (i.e. $\simeq 1 - 2\,\%$ of the supernova rate) in the left panel, which match the cosmic-ray flux at energies as low as $10^{18}\,$eV, in order to provide a maximum neutrino flux for this scenario. The right panel shows the expected neutrino flux if the cosmic-ray flux is matched at energies $> 10^{19}\,$eV, corresponding to a more reasonable occurence rate $n_{\rm s} = 200\,{\rm Gpc^{-3}\,yr^{-1}}$ at $z = 0$. The calculation of the cosmic-ray spectrum considers energy losses during propagation in the intergalactic medium.

The maximum neutrino flux produced by pp interactions lies slightly below the 5-year sensitivity of IceCube-86 and above the 3-year sensitivity of the projected Askaryan Radio Array (ARA). It might thus become detectable in the next decade, depending on the exact

level of contribution of these msec PWNe to the ultra-high energy cosmic ray flux. Note that if the primaries were heavier nuclei and not protons, these estimates would be reduced by an additional factor of a few (see e.g., [89]).

4 Conclusions

This work has examined the possibility that pulsars born with $\sim$ msec periods can accelerate ions to ultra-high energies at the ultra-relativistic termination shock of the pulsar wind. It is motivated mainly by the observation that the Crab nebula, and other pulsar wind nebulae, are able to accelerate pairs at a maximally efficient rate, i.e up to the radiation reaction limit. Known pulsar wind nebulae are however not powerful enough to confine ions up to energies of the order of 10^{20} eV. In this paper, we have therefore constructed a phenomenological model of a much more powerful PWN, with input rotational energy $E_{\rm rot} \sim 10^{52}$ erg and typical spin-down time-scale $t_{\rm sd} \sim 3 \times 10^7$ s; these values correspond to a typical wind luminosity $L_{\rm w} \sim 10^{45}$ erg/s, a typical neutron star magnetic field $B_\star \sim 10^{13}$ G and a typical spin-down rate $\dot{P}/P \sim 5 \times 10^{-8}$ /s.

Our acceleration model assumes that the wind luminosity is substantially converted into particle random kinetic energy through dissipation/acceleration processes around the termination shock, which is supported by strong observational and theoretical arguments that we recalled in Sec. 2.1. We speculate that acceleration to the highest energies can be provided by a relativistic Fermi mechanism at the termination shock, as envisaged in the case of known PWNe.

We find that such PWNe are indeed able to accelerate and confine protons up to energies of the order of the GZK cut-off, for the above fiducial values; synchrotron energy losses are a severe limitation, but their magnitude depends strongly on the parameters of the neutron star. Heavier ions could be accelerated to even larger energies, as they are more easily confined and less affected by synchrotron energy losses. We also find that photo-hadronic losses are not a strong limitation of the acceleration process.

A key assumption of the present work is that ions are injected in the pulsar wind. Such a possibility could be tested by searching for the neutrino signal associated with photopion or photodisintegration losses in the nebula or its surroundings [90–94]. For the fiducial parameters of the sources that we consider, namely a luminosity $L_{\rm p} \sim 10^{45}$ erg/s and spin-down timescale $t_{\rm sd} \sim 3 \times 10^7$ s, the neutrino fluxes peak at high energies $\sim 10^{17} - 10^{18}$ eV, with a maximum diffuse flux that lies slightly below the 5-year sensitivity of IceCube-86 and above the 3-year sensitivity of the projected ARA. It might thus become detectable in the next decade, depending on the exact level of contribution of these msec PWNe to the ultra-high energy cosmic ray flux. One should also search for neutrino signals from galactic sources, as discussed in [90–93, 95]. However, according to the results of Ref. [92], the neutrino flux of Crab-like nebulae should be at most comparable to the atmospheric neutrino background in $10 - 100$ TeV range if the nuclei take up a fraction $\eta_{\rm i} \sim 0.1$ of the pulsar wind luminosity.

Beyond the injection of ions into the pulsar wind, another central assumption of the present work is that a fraction of pulsars are born with a millisecond period. In order to match the cosmic-ray flux at energies $\gtrsim 10^{19.5}$ eV, this fraction should represent $\sim 0.03\,\%$ of the present supernova rate. Although no pulsar with a millisecond period at birth has yet been identified unambiguously, the existence of such objects may be indirectly supported by the recent detections of super-luminous and trans-relativistic supernovae, which can be modelled as engine-driven supernovae, with the inner engine being a young fast spinning

pulsar injecting up to $\sim 10^{52}$ ergs in the remnant on timescales as long as a few years, see e.g. [35, 36, 96]. Actually, it has been suggested that the Crab pulsar itself was born with a 5 msec period, in order to explain the large number of radio-emitting pairs found in the nebula [38]. Clearly, further detailed theoretical work and multi-wavelength follow-up of these supernovae is needed to clarify the possible existence of such objects.

Under the above assumptions, the present work points out a new potential acceleration mechanism of very high energy protons and this is valuable, in our opinion, in the present context of ultra-high energy cosmic ray physics. Indeed, on the theoretical side, there are only a handful of sources capable of accelerating protons up to the GZK cut-off: gamma-ray bursts [8, 9], the most powerful radio-galaxies [13], or magnetars [24]. However, radio-galaxies with a luminosity $\gtrsim 10^{45}$ erg/s, sufficiently large to allow the acceleration of protons to 10^{20} eV, are too rare in the GZK sphere and the arrival directions of the highest energy events do not match any of these, see the discussion in Ref. [97]. Gamma-ray bursts seemingly offer the requisite conditions for the acceleration of protons to ultra-high energies [8], but the non-detection of neutrinos from these sources start to constrain the amount of energy that is injected in cosmic rays, e.g. [98]. Finally, the observation of anisotropies in the arrival directions of high energy events without an anisotropic counterpart at lower energies does point towards the existence of protons at GZK energies [97, 99]. Such anisotropies have been claimed by the Pierre Auger Observatory, at a confidence level of 99 % c.l. [100], and recently by the Telescope Array [101]. In this context, the search for sources of ultra-high energy protons, both on the theoretical and on the experimental level, remains crucial.

Acknowledgments

KK thanks Elena Amato, Pasquale Blasi, Kohta Murase and Ke Fang for very fruitful discussions. This work was supported by the Programme National des Hautes Energies (CNRS).

References

[1] K. Kotera and A. V. Olinto, *The Astrophysics of Ultrahigh Energy Cosmic Rays*, ARAA **49** (Jan., 2011) [arXiv:1101.4256].

[2] A. Letessier-Selvon and T. Stanev, *Ultrahigh energy cosmic rays*, Rev. Mod. Phys. (2011).

[3] R. U. Abbasi et al., *First Observation of the Greisen-Zatsepin-Kuzmin Suppression*, Physical Review Letters **100** (Mar., 2008) 101101–+, [astro-ph/].

[4] **Pierre Auger** Collaboration, J. Abraham et al., *Observation of the suppression of the flux of cosmic rays above* $4 \times 10^{19}\,eV$, Phys. Rev. Lett. **101** (2008) 061101, [arXiv:0806.4302].

[5] L. Sironi, A. Spitkovsky, and J. Arons, *The Maximum Energy of Accelerated Particles in Relativistic Collisionless Shocks*, ApJ **771** (July, 2013) 54, [arXiv:1301.5333].

[6] B. Katz, R. Budnik, and E. Waxman, *The energy production rate and the generation spectrum of UHECRs*, Journal of Cosmology and Astro-Particle Physics **3** (Mar., 2009) 20–+, [arXiv:0811.3759].

[7] A. Bykov, N. Gehrels, H. Krawczynski, M. Lemoine, G. Pelletier, and M. Pohl, *Particle Acceleration in Relativistic Outflows*, Sp. Sc. Rev. **173** (Nov., 2012) 309–339, [arXiv:1205.2208].

[8] E. Waxman, *Cosmological Origin for Cosmic Rays above 10 19 eV*, ApJl **452** (Oct., 1995) L1+, [astro-ph/].

[9] M. Vietri, *The Acceleration of Ultra–High-Energy Cosmic Rays in Gamma-Ray Bursts*, ApJ **453** (Nov., 1995) 883–+, [astro-ph/].

[10] D. Gialis and G. Pelletier, *Which acceleration process for ultra high energy cosmic rays in gamma ray bursts?*, A&A **425** (Oct., 2004) 395–403, [astro-ph/].

[11] E. Waxman, *High-Energy Particles from γ-Ray Bursts*, in Phys Astrophys of UHECRs (M. Lemoine and G. Sigl, eds.), vol. 576 of Lecture Notes in Physics, Berlin Springer Verlag, p. 122, 2001.

[12] C. D. Dermer and S. Razzaque, *Acceleration of Ultra-high-energy Cosmic Rays in the Colliding Shells of Blazars and Gamma-ray Bursts: Constraints from the Fermi Gamma-ray Space Telescope*, ApJ **724** (Dec., 2010) 1366–1372, [arXiv:1004.4249].

[13] J. P. Rachen and P. L. Biermann, *Extragalactic Ultra-High Energy Cosmic-Rays - Part One - Contribution from Hot Spots in Fr-II Radio Galaxies*, A&A **272** (May, 1993) 161–+, [astro-ph/].

[14] Y. A. Gallant and A. Achterberg, *Ultra-high-energy cosmic ray acceleration by relativistic blast waves*, MNRAS **305** (May, 1999) L6–L10, [astro-ph/].

[15] R. A. Chevalier, *Was SN 1054 A Type II Supernova?*, in Supernovae (D. N. Schramm, ed.), vol. 66 of Astrophysics and Space Science Library, p. 53, 1977.

[16] R. A. Chevalier and C. Fransson, *Pulsar nebulae in supernovae*, ApJ **395** (Aug., 1992) 540–552.

[17] B. M. Gaensler and P. O. Slane, *The Evolution and Structure of Pulsar Wind Nebulae*, ARAA **44** (Sept., 2006) 17–47, [astro-ph/].

[18] A. M. Atoyan and F. A. Aharonian, *On the mechanisms of gamma radiation in the Crab Nebula*, MNRAS **278** (Jan., 1996) 525–541.

[19] J. Bednarz and M. Ostrowski, *Energy Spectra of Cosmic Rays Accelerated at Ultrarelativistic Shock Waves*, Physical Review Letters **80** (May, 1998) 3911–3914, [astro-ph/].

[20] J. G. Kirk, A. W. Guthmann, Y. A. Gallant, and A. Achterberg, *Particle Acceleration at Ultrarelativistic Shocks: An Eigenfunction Method*, ApJ **542** (Oct., 2000) 235–242, [astro-ph/].

[21] A. Achterberg, Y. A. Gallant, J. G. Kirk, and A. W. Guthmann, *Particle acceleration by ultrarelativistic shocks: theory and simulations*, MNRAS **328** (Dec., 2001) 393–408, [astro-ph/].

[22] M. Lemoine and G. Pelletier, *Particle Transport in Tangled Magnetic Fields and Fermi Acceleration at Relativistic Shocks*, ApJl **589** (June, 2003) L73–L76, [astro-ph/].

[23] U. Keshet and E. Waxman, *Energy Spectrum of Particles Accelerated in Relativistic Collisionless Shocks*, Physical Review Letters **94** (Mar., 2005) 111102, [astro-ph/].

[24] J. Arons, *Magnetars in the Metagalaxy: An Origin for Ultra-High-Energy Cosmic Rays in the Nearby Universe*, ApJ **589** (June, 2003) 871–892, [astro-ph/].

[25] M. Hoshino, J. Arons, Y. A. Gallant, and A. B. Langdon, *Relativistic magnetosonic shock waves in synchrotron sources - Shock structure and nonthermal acceleration of positrons*, ApJ **390** (May, 1992) 454–479.

[26] Y. A. Gallant and J. Arons, *Structure of relativistic shocks in pulsar winds: A model of the wisps in the Crab Nebula*, ApJ **435** (Nov., 1994) 230–260.

[27] A. Spitkovsky and J. Arons, *Time Dependence in Relativistic Collisionless Shocks: Theory of the Variable "Wisps" in the Crab Nebula*, ApJ **603** (Mar., 2004) 669–681, [astro-ph/0402123].

[28] A. Venkatesan, M. C. Miller, and A. V. Olinto, *Constraints on the Production of Ultra–High-Energy Cosmic Rays by Isolated Neutron Stars*, ApJ **484** (July, 1997) 323–+, [astro-ph/].

[29] P. Blasi, R. I. Epstein, and A. V. Olinto, *Ultra-High-Energy Cosmic Rays from Young Neutron Star Winds*, ApJ Letters **533** (Apr., 2000) L123–L126, [astro-ph/].

[30] K. Fang, K. Kotera, and A. V. Olinto, *Newly Born Pulsars as Sources of Ultrahigh Energy Cosmic Rays*, The Astrophysical Journal **750** (May, 2012) 118, [arXiv:1201.5197].

[31] K. Fang, K. Kotera, and A. V. Olinto, *Ultrahigh energy cosmic ray nuclei from extragalactic pulsars and the effect of their Galactic counterparts*, JCAP **3** (Mar., 2013) 10, [arXiv:1302.4482].

[32] D. Kasen and L. Bildsten, *Supernova Light Curves Powered by Young Magnetars*, ApJ **717** (July, 2010) 245–249, [arXiv:0911.0680].

[33] S. E. Woosley, *Bright Supernovae from Magnetar Birth*, ApJ Letters **719** (Aug., 2010) L204–L207, [arXiv:0911.0698].

[34] L. Dessart, D. J. Hillier, R. Waldman, E. Livne, and S. Blondin, *Super-luminous supernovae: 56Ni power versus magnetar radiation*, ArXiv e-prints (Aug., 2012) [arXiv:1208.1214].

[35] K. Kotera, E. S. Phinney, and A. V. Olinto, *Signatures of pulsars in the light curves of newly formed supernova remnants*, MNRAS (May, 2013) [arXiv:1304.5326].

[36] B. D. Metzger, I. Vurm, R. Hascoët, and A. M. Beloborodov, *Ionization break-out from millisecond pulsar wind nebulae: an X-ray probe of the origin of superluminous supernovae*, MNRAS **437** (Jan., 2014) 703–720, [arXiv:1307.8115].

[37] R. M. Quimby, *Superluminous Supernovae*, in IAU Symposium, vol. 279 of IAU Symposium, pp. 22–28, Sept., 2012.

[38] A. M. Atoyan, *Radio spectrum of the Crab nebula as an evidence for fast initial spin of its pulsar*, A&A **346** (June, 1999) L49–L52, [astro-ph/9905204].

[39] X.-Y. Wang, S. Razzaque, P. Mészáros, and Z.-G. Dai, *High-energy cosmic rays and neutrinos from semirelativistic hypernovae*, Phys. Rev. D **76** (Oct., 2007) 083009–+, [arXiv:0705.0027].

[40] R.-Y. Liu and X.-Y. Wang, *Energy Spectrum and Chemical Composition of Ultrahigh Energy Cosmic Rays from Semi-relativistic Hypernovae*, ApJ **746** (Feb., 2012) 40, [arXiv:1111.6256].

[41] S. Chakraborti, A. Ray, A. M. Soderberg, A. Loeb, and P. Chandra, *Ultra-high-energy cosmic ray acceleration in engine-driven relativistic supernovae*, Nature Communications **2** (Feb., 2011) [arXiv:1012.0850].

[42] M. J. Rees and J. E. Gunn, *The origin of the magnetic field and relativistic particles in the Crab Nebula*, MNRAS **167** (Apr., 1974) 1–12.

[43] W. Bednarek and R. J. Protheroe, *Contribution of nuclei accelerated by gamma-ray pulsars to cosmic rays in the Galaxy*, Astroparticle Physics **16** (Feb., 2002) 397–409, [astro-ph/].

[44] C. F. Kennel and F. V. Coroniti, *Confinement of the Crab pulsar's wind by its supernova remnant*, ApJ **283** (Aug., 1984) 694–709.

[45] C. F. Kennel and F. V. Coroniti, *Magnetohydrodynamic model of Crab nebula radiation*, ApJ **283** (Aug., 1984) 710–730.

[46] S. Komissarov and Y. Lyubarsky, *MHD Simulations of Crab's Jet and Torus*, Ap & SS **293** (Sept., 2004) 107–113.

[47] O. Porth, S. S. Komissarov, and R. Keppens, *Solution to the sigma problem of pulsar wind nebulae*, MNRAS **431** (Apr., 2013) L48–L52, [arXiv:1212.1382].

[48] B. D. Metzger, D. Giannios, and S. Horiuchi, *Heavy nuclei synthesized in gamma-ray burst outflows as the source of ultrahigh energy cosmic rays*, MNRAS **415** (Aug., 2011) 2495–2504, [arXiv:1101.4019].

[49] L. Del Zanna, E. Amato, and N. Bucciantini, *Axially symmetric relativistic MHD simulations of Pulsar Wind Nebulae in Supernova Remnants. On the origin of torus and jet-like features*, A&A **421** (July, 2004) 1063–1073, [astro-ph/].

[50] J. D. Gelfand, P. O. Slane, and W. Zhang, *A Dynamical Model for the Evolution of a Pulsar Wind Nebula Inside a Nonradiative Supernova Remnant*, ApJ **703** (Oct., 2009) 2051–2067, [arXiv:0904.4053].

[51] N. Bucciantini, J. Arons, and E. Amato, *Modelling spectral evolution of pulsar wind nebulae inside supernova remnants*, MNRAS **410** (Jan., 2011) 381–398.

[52] J. D. Gelfand, P. O. Slane, and T. Temim, *The properties of the progenitor, neutron star, and pulsar wind in the supernova remnant Kes 75*, Astronomische Nachrichten **335** (Mar., 2014) 318–323.

[53] J. Martin, D. F. Torres, A. Cillis, and E. de Oña Wilhelmi, *Is there room for highly magnetized pulsar wind nebulae among those non-detected at TeV?*, MNRAS **443** (Sept., 2014) 138–145, [arXiv:1406.1344].

[54] S. S. Komissarov, *Magnetic dissipation in the Crab nebula*, MNRAS **428** (Jan., 2013) 2459–2466, [arXiv:1207.3192].

[55] F. V. Coroniti, *Magnetically striped relativistic magnetohydrodynamic winds - The Crab Nebula revisited*, ApJ **349** (Feb., 1990) 538–545.

[56] T. Chiueh, Z.-Y. Li, and M. C. Begelman, *A Critical Analysis of Ideal Magnetohydrodynamic Models for Crab-like Pulsar Winds*, ApJ **505** (Oct., 1998) 835–843.

[57] I. Contopoulos and D. Kazanas, *Toward Resolving the Crab σ-Problem: A Linear Accelerator?*, ApJ **566** (Feb., 2002) 336–342, [astro-ph/].

[58] J. G. Kirk, Y. Lyubarsky, and J. Petri, *The Theory of Pulsar Winds and Nebulae*, in Astrophysics and Space Science Library (W. Becker, ed.), vol. 357 of Astrophysics and Space Science Library, p. 421, 2009. astro-ph/.

[59] Y. Lyubarsky, *A New Mechanism for Dissipation of Alternating Fields in Poynting-dominated Outflows*, ApJL **725** (Dec., 2010) L234–L238, [arXiv:1012.1411].

[60] M. Lemoine and G. Pelletier, *On electromagnetic instabilities at ultra-relativistic shock waves*, MNRAS **402** (Feb., 2010) 321–334, [arXiv:0904.2657].

[61] M. Lemoine and G. Pelletier, *Dispersion and thermal effects on electromagnetic instabilities in the precursor of relativistic shocks*, MNRAS **417** (Oct., 2011) 1148–1161, [arXiv:1102.1308].

[62] M. Lemoine, G. Pelletier, and B. Revenu, *On the Efficiency of Fermi Acceleration at Relativistic Shocks*, ApJl **645** (July, 2006) L129–L132, [astro-ph/].

[63] M. Lemoine, G. Pelletier, L. Gremillet, and I. Plotnikov, *Current-driven filamentation upstream of magnetized relativistic collisionless shocks*, Mont. Not. Roy. Astron. Soc. (Mar., 2014) [arXiv:1401.7166].

[64] G. Pelletier, M. Lemoine, and A. Marcowith, *On Fermi acceleration and magnetohydrodynamic instabilities at ultra-relativistic magnetized shock waves*, MNRAS **393** (Feb., 2009) 587–597, [arXiv:0807.3459].

[65] F. C. Michel, *Theory of pulsar magnetospheres*, Reviews of Modern Physics **54** (Jan., 1982) 1–66.

[66] F. C. Michel, *Magnetic structure of pulsar winds*, ApJ **431** (Aug., 1994) 397–401.

[67] J. G. Kirk and O. Skjæraasen, *Dissipation in Poynting-Flux-dominated Flows: The σ-Problem of the Crab Pulsar Wind*, ApJ **591** (July, 2003) 366–379, [astro-ph/].

[68] A. Barnes and J. D. Scargle, *Collisionless Damping of Hydromagnetic Waves in Relativistic Plasma. Weak Landau Damping*, ApJ **184** (Aug., 1973) 251–270.

[69] Y. E. Lyubarsky, *The termination shock in a striped pulsar wind*, MNRAS **345** (Oct., 2003) 153–160, [astro-ph/].

[70] J. Pétri and Y. Lyubarsky, *Magnetic reconnection at the termination shock in a striped pulsar wind*, A&A **473** (Oct., 2007) 683–700.

[71] L. Sironi and A. Spitkovsky, *Acceleration of Particles at the Termination Shock of a Relativistic Striped Wind*, ApJ **741** (Nov., 2011) 39, [arXiv:1107.0977].

[72] N. F. Camus, S. S. Komissarov, N. Bucciantini, and P. A. Hughes, *Observations of 'wisps' in magnetohydrodynamic simulations of the Crab Nebula*, MNRAS **400** (Dec., 2009) 1241–1246, [arXiv:0907.3647].

[73] J. A. Hibschman and J. Arons, *Pair Production Multiplicities in Rotation-powered Pulsars*, ApJ **560** (Oct., 2001) 871–884, [astro-ph/0107209].

[74] A. N. Timokhin, *Time-dependent pair cascades in magnetospheres of neutron stars - I. Dynamics of the polar cap cascade with no particle supply from the neutron star surface*, MNRAS **408** (Nov., 2010) 2092–2114, [arXiv:1006.2384].

[75] S. P. Reynolds and R. A. Chevalier, *Evolution of pulsar-driven supernova remnants*, ApJ **278** (Mar., 1984) 630–648.

[76] D. F. Torres, A. Cillis, J. Martín, and E. de Oña Wilhelmi, *Time-dependent modeling of TeV-detected, young pulsar wind nebulae*, Journal of High Energy Astrophysics **1** (May, 2014) 31–62, [arXiv:1402.5485].

[77] P. Goldreich and W. H. Julian, *Pulsar Electrodynamics*, ApJ **157** (Aug., 1969) 869–+.

[78] A. Aab and et al. (Pierre Auger Collaboration), *Depth of maximum of air-shower profiles at the Pierre Auger Observatory. II. Composition implications*, Phys. Rev. D **90** (Dec., 2014) 122006.

[79] R. U. Abbasi and et al. (Telescope Array Collaboration), *Study of Ultra-High Energy Cosmic Ray composition using Telescope Array's Middle Drum detector and surface array in hybrid mode*, Astroparticle Physics **64** (Apr., 2015) 49–62, [arXiv:1408.1726].

[80] R. Abbasi, J. Bellido, J. Belz, V. de Souza, W. Hanlon, D. Ikeda, J. P. Lundquist, P. Sokolsky, T. Stroman, Y. Tameda, Y. Tsunesada, M. Unger, A. Yushkov for the Pierre Auger Collaboration, and the Telescope Array Collaboration, *Report of the Working Group on the Composition of Ultra High Energy Cosmic Rays*, ArXiv e-prints (Mar., 2015) [arXiv:1503.0754].

[81] J. Niemiec, M. Ostrowski, and M. Pohl, *Cosmic-Ray Acceleration at Ultrarelativistic Shock Waves: Effects of Downstream Short-Wave Turbulence*, ApJ **650** (Oct., 2006) 1020–1027, [astro-ph/].

[82] R. D. Blandford and C. F. McKee, *Fluid dynamics of relativistic blast waves*, Physics of Fluids **19** (Aug., 1976) 1130–1138.

[83] F. W. Stecker and M. H. Salamon, *Photodisintegration of Ultra-High-Energy Cosmic Rays: A New Determination*, ApJ **512** (Feb., 1999) 521–526, [astro-ph/].

[84] J. P. Rachen and P. Mészáros, *Photohadronic neutrinos from transients in astrophysical sources*, Phys. Rev. D **58** (Dec., 1998) 123005, [astro-ph/9802280].

[85] R. Abbasi et al., *The IceCube Neutrino Observatory II: All Sky Searches: Atmospheric, Diffuse and EHE*, arXiv:1111.2736.

[86] **JEM-EUSO** Collaboration, J. Adams et al., *The JEM-EUSO Mission: Status and Prospects in 2011*, arXiv:1204.5065.

[87] P. Allison, J. Auffenberg, R. Bard, J. Beatty, D. Besson, et al., *Design and Initial Performance of the Askaryan Radio Array Prototype EeV Neutrino Detector at the South Pole*, Astropart.Phys. **35** (2012) 457–477, [arXiv:1105.2854].

[88] **Pierre Auger Collaboration** Collaboration, A. Aab et al., *The Pierre Auger Observatory: Contributions to the 33rd International Cosmic Ray Conference (ICRC 2013)*, arXiv:1307.5059.

[89] K. Murase and J. F. Beacom, *Neutrino background flux from sources of ultrahigh-energy cosmic-ray nuclei*, Phys. Rev. D **81** (June, 2010) 123001–+, [arXiv:1003.4959].

[90] W. Bednarek and R. J. Protheroe, *Gamma Rays and Neutrinos from the Crab Nebula Produced by Pulsar Accelerated Nuclei*, Phys. Rev. Lett. **79** (Oct., 1997) 2616–2619, [astro-ph/9704186].

[91] W. Bednarek, *Extragalactic neutrino background from very young pulsars surrounded by supernova envelopes*, Astron. Astrophys. **378** (Oct., 2001) L49–L52, [astro-ph/0109225].

[92] W. Bednarek, *Neutrinos from the pulsar wind nebulae*, Astron. Astrophys. **407** (Aug., 2003) 1–6, [astro-ph/0305430].

[93] E. Amato, D. Guetta, and P. Blasi, *Signatures of high energy protons in pulsar winds*, Astron. Astrophys. **402** (May, 2003) 827–836, [astro-ph/0302121].

[94] K. Fang, K. Kotera, K. Murase, and A. V. Olinto, *Testing the newborn pulsar origin of ultrahigh energy cosmic rays with EeV neutrinos*, Phys. Rev. D **90** (Nov., 2014) 103005, [arXiv:1311.2044].

[95] K. Fang, *High-Energy Neutrino Signatures of Newborn Pulsars In the Local Universe*, ArXiv e-prints (Nov., 2014) [arXiv:1411.2174].

[96] K. Murase, K. Kashiyama, K. Kiuchi, and I. Bartos, *Gamma-Ray and Hard X-Ray Emission from Pulsar-Aided Supernovae as a Probe of Particle Acceleration in Embryonic Pulsar Wind Nebulae*, ArXiv e-prints: 1411.0619 (Nov., 2014) [arXiv:1411.0619].

[97] M. Lemoine and E. Waxman, *Anisotropy vs chemical composition at ultra-high energies*, J. Cosm. Astropart. Phys. **11** (Nov., 2009) 9, [arXiv:0907.1354].

[98] R. Abbasi, Y. Abdou, T. Abu-Zayyad, M. Ackermann, J. Adams, J. A. Aguilar, M. Ahlers, D. Altmann, K. Andeen, J. Auffenberg, and et al., *An absence of neutrinos associated with cosmic-ray acceleration in γ-ray bursts*, Nature **484** (Apr., 2012) 351–354, [arXiv:1204.4219].

[99] R.-Y. Liu, A. M. Taylor, M. Lemoine, X.-Y. Wang, and E. Waxman, *Constraints on the Source of Ultra-high-energy Cosmic Rays Using Anisotropy versus Chemical Composition*, Astrophys. J. **776** (Oct., 2013) 88, [arXiv:1308.5699].

[100] Pierre Auger Collaboration, P. Abreu, M. Aglietta, E. J. Ahn, I. F. M. Albuquerque, D. Allard, I. Allekotte, J. Allen, P. Allison, J. Alvarez Castillo, and et al., *Anisotropy and chemical composition of ultra-high energy cosmic rays using arrival directions measured by the Pierre Auger Observatory*, J. Cosm. Astropart. Phys. **6** (June, 2011) 22, [arXiv:1106.3048].

[101] The Telescope Array Collaboration, R. U. Abbasi, and et al., *Indications of Intermediate-Scale Anisotropy of Cosmic Rays with Energy Greater Than 57 EeV in the Northern Sky Measured with the Surface Detector of the Telescope Array Experiment*, ArXiv e-prints (Apr., 2014) [arXiv:1404.5890].